SEM-EDS characterization of historic mortar as a tool in archaeometric study: an updated analytical protocol tested on the Roman theatre of Aosta (NW Italy).

SEM-EDS characterization of historic mortar as a tool in archeologic study: an updated analytical protocol tested on the Roman Theater of Aosta (NW Italy)

F. Gambino[1]*, Glarey A.[1], Cossio R.[1], L. Appolonia[1], d'Atri A.[1], A. Borghi[1]

[1] Department of Earth Sciences, University of Turin, Via Valperga Caluso 35, Torino 10125, Italy

Corresponding Author: Alessandro.borghi@unito.it

Abstract

The archaeometric study of ancient mortars can provide important information relating to the raw materials used and their provenance. A mineralogical and petrographic study based on optical and electron microscopy on mortars from the Roman theater of Aosta (NW Italy) was carried out. The construction of the theater is believed to have taken place a few decades after the foundation of *Augusta Praetoria*, the ancient city of Aosta, in 25 BC. Both original and mortars belonging to four different subsequent restoration interventions were studied. It was possible to detect the areas of origin of the materials used for the historical mortars, which were of local, being characterized by abundant metamorphic minerals. X-ray element maps were also created to better define the distribution of aggregate, binder and porosity. The characterization of the binder was obtained by creating two-dimensional maps of the hydraulic index. These made it possible to distinguish aerial binders from the Roman era and hydraulic mortars for subsequent restorations

Key word: historic mortar, SEM – EDS facility, X-ray maps, Aosta (NW Italy)

1. Introduction

Mortars, since ancient times, are an artificial and man-made product made up of natural materials typically obtained by the firing of a carbonate or gypsum. By this process, the *binder* forms and, only after the mixing with an *aggregate* and *water*, it hardens becoming a mortar (Pecchioni et al., 2018).

Mortars are used to embed masonry units as well as wall finishing materials both internally (plaster) and externally (render). Mud was the first material adopted for these purposes and, although it is still used in earth construction, it is neither strong nor durable. To satisfy the demand for dependable structures, stronger and more durable binders have developed, the main ones being based on lime, cement and gypsum (Ingham, 2013).

Currently, according to NORMA UNI 10924 (2001), mortars are defined as a mixture of binders (organic or inorganic), aggregates (mainly of fine grain size) and water, to which it is possible to

add one or more organic or inorganic additives, in order to improve and/or control the laying conditions of the mix, its physical characteristics (e.g. porosity, water permeability) and mechanical characteristics as resistance, deformability, adherence to surfaces, etc.

The use of mortars seems to have origin in prehistoric times. The discovery probably occurred as the result of an accidental event: the firing of a carbonate rock. It would have been reduced to a powder by heating (calcination process) then extinguished with water and then hardened in the air (Schiele and Berens, 1976) .

In ancient times, people used different types of both binders and mortars for different purposes; these materials were known in Asia, Mesopotamia, Near East and Egypt. The Minoan civilization handed down to the Greeks the art of lime production that was in turn transmitted to the Etruscans. The Romans increased the Greeks' knowledge of mortars and began to spread out the use of these materials, improving their physical and chemical characteristics.

Thanks to the Romans, their writings and the study of the several Roman buildings still in good conditions, the advanced techniques of mortar production are nowadays known.

With the Industrial Revolution the first *cement*, called “Portland”, was introduced between the end of the 18th century and the beginning of the 19th century (the name Portland derives from the similarity with the rocks coming from the homonymous town in the southern peninsula of Great Britain).

Today's cement is obtained by baking mixtures of limestone and clay (*artificial cement*) or, rarely, marly limestone (*natural cement*) at very high temperatures (1450°C) allowing the complete combination of calcium oxide with silica and alumina in the molten state. The resulting material is called clinker.

Nowadays, several techniques are used to characterize mortars: wet chemical analysis, instrumental methods for characterization of organic and inorganic materials as thermal analysis (DTA, TGA, DSC) (Pires and Cruz, 2007; Moropoulou et al., 1995) and infra-red spectroscopy (FTIR) (Derrik et al., 1999), physical and mechanical testing for durability and performance assessment respectively, radiocarbon dating (this technique has recently allowed to date mortars to an accuracy of about 30 years) and X-ray diffraction (XRD) (NORMA UNI EN 13925-1, 2006; NORMA UNI EN 13925-2, 2006; NORMA UNI EN 13925-3, 2006). Other instrumental techniques for the analysis of organic materials are also adopted (gas chromatography with mass spectrometry; ion, liquid and thin layer chromatography).

For this topic, a petrographic approach was adopted involving optical microscopy (OM) and Electron Microscopy with X-ray analysis (SEM-EDS).

Mortars characterization has been performed by combining macroscopic observations, minero-petrographic and micro-chemical techniques as shown in several works (Cantù et al., 2015; Lezzerini et al., 2017; 2018; Miriello et al., 2010; Ricciardi et al., 2007).

The minero-petrographic approach was applied to mortar samples belonging to the Ancient Roman Theatre of Aosta (Aosta Valley, Italy). These samples represent the target of a new and original analytical protocol for the study of mortars based on optical microscopy, SEM-EDS analysis and automated acquisition and semi-automated processing of quantitative multi-elemental X-ray maps. Mineral phases of the aggregate and the composition of the binder are classified in a representative area. The described methodology represents an upgrade of the standard archaeometric and minero-petrographic procedure typically performed by optical microscope and by SEM-EDS and it allows to investigate the composition of the binder and the aggregate, provenance of raw materials, "dating" of mortar samples and comparison of different samples.

In addition, by simple algebraic operations, pixel by pixel full quantification of each EDS spectrum of the elemental maps (expressed as oxides) was performed in order to calculate the distribution of Hydraulicity Index (HI), with its statistical error, within the investigated domains. Interestingly, also within altered mortars, the HI values can be precisely defined.

The outcome of this methodology consists in the constitution of an analytic protocol that can be applied for every kind of mortar, plaster and cement by a minero-petrographic point of view.

2. The Roman Theatre of Aosta

The focus of this research is the study of mortars of the Roman Theatre of Aosta (**Fig. 1**). The analyzed samples are of roman age as well as different subsequent restoration phases.

The city of Aosta, the ancient Augusta Prætoria, was founded in the 25 B.C., whereas the buildings for public performances such as the Theatre and the Amphitheatre, located in the north-eastern corner of the town plan, were built a few decades later, as the remains of pre-existing buildings discovered in the area demonstrate.

The Theatre is one of the masterpieces of the Roman provincial architecture of the High Empire. Besides the façade, the most visible and easily recognizable architectural component inside the Theatre Roman Area is certainly the cavea. Its remaining lower semicircular steps (ima cavea) and præcinctiones, are today entirely covered with blocks of local travertine.

The pulpitum, the curved and rectangular architectural component that precedes the scæna originally clad with marble of different colours, was then reconstructed with cement-bounded terracotta bricks; this technique was used in the Aosta Valley for other architectural restorations from the end of the 19th century onward.

The masonry structure of the area behind the cavea is largely constituted by fluvial pebbles, whole or split in half, of quartzite, schist and granite. Travertine was also widely used. Rarely grey marble, conglomerate and brick were also employed. Instead, conglomerate with different granulometry and travertine was adopted for the façade. During several restorations the use of the same materials has been encouraged. In some cases, the intervention is perfectly recognizable. All these aspects are observable in **Fig. 2**.

The combination of different materials, along with the overlapping construction techniques, maintenance and restoration phases, confer to the Roman Theatre Area a very heterogeneous aspect. Indeed, it is characterized by several building material and, for this reason, it shows very diversified preservation conditions (Pedelì, 2009).

Up to the 18th century, the whole knowledge about the original function of the building was lost and its remains were recognized only recently. Carlo Promis, Inspector of Monuments of Antiquity of the State Regions in 1837, performed the first investigations on the monument. From 1838 the Roman Theatre was then studied and surveyed by scientific methods. In 1864 some excavations revealed a series of walls, while in the 20s of the twentieth century an initial arrangement of the monument started by the demolition of the houses that surrounded it. However, it was completely brought to light between 1933 and 1941, when important restoration and integration works were carried out.

Over the last century, the monument has undergone numerous restorations (e.g. different walls of the Theater). The parts of the residual masonry of the ancient theatrical structure, discovered in the 1930's and which have not been subject of subsequent reconstructions, can be attributed to the so-called “original phase”. The mortars of this phase macroscopically appear very degraded, disintegrated and often almost pulverised.

The first phase of restoration was carried out in the 1930's and involved a major renovation of the masonry, which was rebuilt in its missing parts. This is the most extensive and homogeneous restoration work recognizable in the theatre area and is the only one that also affects the upper part of the walls. The first restoration work was followed by others of minor importance, clearly recognizable in the vertical stratigraphy of the masonry. This phase, conventionally called "second

restoration phase", is characterized by a limited extension and non-homogeneity of both the materials and techniques adopted. From a stratigraphic point of view, and following the heterogeneous interventions described above, there is a "third phase of restoration", which is widespread and uniform. The last recognizable phase is represented by a series of occasional reconstructions in cement mortar carried out at different times in order to close small open voids in the facing. As for the second phase, this "fourth restoration phase" does not show a unitary design of intervention but seems to be the result of extraordinary maintenance following localized degradation phenomena

3. Geological Setting

The petrographic study of mortars, in particular of aggregates, when compared with regional geology, allows to obtain important information on the source areas of the raw materials with which they were made. The study of the raw materials used in the original and restoration mortars cannot therefore ignore the geological knowledge of the surrounding areas.

The Roman Theatre stay in Aosta town, the regional capital of Aosta Valley. The city of Aosta is located within the Combin Zone (Giusti et al., 2004) (**Fig.3**) which represents the metamorphic product of the Ligurian-Piedmontese ocean originally interposed in the Mesozoic age between the Paleo-European and Insubric continental margins (e.g., Dal PIaz, 1999; Beltrando et al., 2010). The Piedmontese Zone includes two main tectonic units, called Zermatt-Saas Zone (lower) and Combin Zone (upper). The Zermatt-Saas Zone is dominated by ophiolites deriving from a basic and ultra-basic protolite. The metamorphic evolution is characterized by a first event developed under eclogitic facies of Eocene age, followed by a retrograde event in greenschist facies conditions (Beltrando et al., 2010; Ernst and Dal Piaz, 1978). The upper Piedmont nappe (Combin Zone) consists mainly of Mesozoic metasediments (calcschist and impure marble) interbedded with tabular levels of metabasites (prasinite) and slices of serpentinite and minor meta-gabbro. The Combin Zone shows metamorphic relict in blueschist facies conditions, strongly retrogressed to greenschist facies in the Eocene-Oligocene age (De Giusti et al., 2004; Dal Piaz, 1999).

Near the city of Aosta, other important geological units of the Alpine chain also outcrop. The Austroalpine domain consists of the Sesia Lanzo Zone, which extends in the lower valley, between Verres and the Canavese Line, and represents the innermost (eastern) unit of the Alpine chain. In addition to the Sesia Lanzo Zone, the Austroalpine Domain also includes a group of external elements (Dent Blanche nappe of Argand s.l.). They are divided into eclogitic lower units (M. Emilius, Glacier-Rafray, Chatillon, Etirol-Levatz, etc.) and non-eclogitic upper units (Dent Blanche s.s., M. Mary, Pillonet): the former is located between the Combin and Zermatt-Saas units, or

within the Zermatt-Saas unit, the latter lies over the Piedmontese Zone, at the same structural level as the Sesia-Lanzo Zone (De Giusti et al., 2004). All tectonic units referred to the Austroalpine domain consist of continental – derived pre-Alpine basement with minor slices of Mesozoic carbonate cover (Roisan Zone). The Pennidic Domain is dominated by the composite nappe of the Great St. Bernard and by the Internal Pennidic Massifs of Monte Rosa and Gran Paradiso, tectonically overthrusted by the main ophiolitic units of the Piedmont Zone.

The Gran Paradiso and Monte Rosa nappes represents the metamorphic product of pre-Mesozoic continental units equilibrated under eclogite – facies metamorphic conditions. They mainly consist of mono- and poly-metamorphic silicate-bearing rocks as micaschist and orthogneiss and minor meta-carbonate cover of Mesozoic age (De Giusti et al., 2004; Malusà et al., 2005).

The Great St. Bernard composite nappe consists of a polymetamorphic continental basement, a monometamorphic basement of Carboniferous -Permian age and a mainly meta-carbonate cover of Mesozoic age. In the more external position of the Pennidic domain, the Sion–Courmayeur Zone outcrops (Elter and Elter, 1965), interpreted as an outer oceanic unit with respect to the Piedmont Zone (Loprieno et al., 2011, with references). In the Aosta Valley, the Sion–Courmayeur Zone consists of two main geological units: the Roignais Versoyen Unit and the Brèches de Tarentaise Unit. The first is composed of oceanic metasediments, metabasites and serpentinitized lherzolites of Mesozoic age. The presence in the metabasites of high-pressure metamorphic assemblages is reported by (Cannic et al., 1996; Beltrando et al., 2010) and references therein.

Finally, the Helvetic Domain is a large tectonic unit that occurs north-west of Pennidic Front and crop out in the Italian territory only marginally, forming the massif of Mont Blanc. It consists of a continental basement, characterized by polymetamorphic schists, orthogneiss and Permian granite, and Mesozoic units represented by weakly metamorphosed predominantly carbonate successions (Von Raumer, 1987).

4. Materials and Methods

4.1 The samples

Forty-two samples of mortars were taken by a chisel during two different restoration campaign performed in 2008 and in 2009 and described in (Appolonia et al., 2010). The complete list of analyzed samples is reported in **Table 1**.

A detailed location of the sampling is given in **Fig.4a**. Thin sections of these samples were prepared in order to perform observation by optical microscope and SEM- EDS analyses.

All samples have been observed by optical microscope. Nevertheless, eight samples, belonging to first and second campaign of restoration, were selected to apply the analytical protocol described in the following paragraph.

The original mortars of Roman age were chosen based on their representativeness and on the quantity of binder still present. Indeed, of the binder of these samples showed a poor state of preservation to the point that, in some cases, the binder resulted almost absent. They are the following: AAM01, AAM17, AAM25, AAM37.

Mortars of restoration phases are selected from the same wall 6 represented in **Fig. 4b** to maintain a coherence between sampling and analysis. They are the following: AAM33, AAM34, AAM35, AAM36.

4.2 Analytical protocol

A new analytical protocol for the study of these geomaterials has been developed and tested on the above-mentioned samples. It consists of a combination of standard petrographic tools and an innovative semi-automated investigative method by quantitative X-ray mapping that, following five steps, leads to a complete characterization of mortar.

The preliminary thin section studies performed by optical microscope are useful to get basic information on the main characteristics and properties of these artificial materials. Data obtained by SEM-EDS and X-ray mapping complement the information obtained by the petrographic studies (Karkanas, 2007; Bany Yaseen et al., 2013). SEM-EDS analysis allows to perform elemental analysis of samples and is used for characterization of textural and compositional interrelationships of mortar components. Quantitative X-ray mapping, when used, furnish the point-by-point chemical composition of the analyzed area of the thin section.

This analytical approach allows to get some interesting archaeometric parameter. At first, it allows to recognize the type of binder and the nature of the aggregate providing many answers about supply areas, variation of raw materials over the time, network/transportation systems, development and production processes. Consequently, it is possible to understand which kind of stone has been used to produce the lime, the binder/aggregate ratio, the geographic and geologic origin of the aggregate and its composition.

4.3 Composition of the mineralogical phases

The data concerning the chemical composition of the mineralogical phases present within the analyzed mortars were obtained through the use of an energy dispersion microprobe (EDS) Link

System equipped with a scanning electron microscope. The operating conditions used were: potential difference = 15Kv, beam current = 800pA, working distance = 10mm, counting times = 25s. Cobalt was used as a reference standard and the analyzed sections were previously polished and metallized with graphite. The mineral analyzes were acquired using the INCA 300 operating system and were recalculated using the MINSORT software (Petrakakis and Dietrich, 1985).

The values reported in the text of the various elements making up the mineralogical phases are to be considered expressed in atoms per unit of formula (a.p.u.f.). The acronyms of the minerals used in the text are taken from (Whitney and Evans, 2010)

4.4 X-ray maps

The maps were acquired by means of the SEM-EDS system installed in the laboratories of the Department of Earth Sciences in Turin using the AZTEC operating system of Oxford Instruments. Digital maps are made up of numerical matrices where in each pixel the number of X-rays detected for a particular characteristic energy interval for each mapped element is reported. TruMap AZtec© has developed an algorithm for automatic peak deconvolution and background removal, thus allowing the real-time acquisition of compositional maps where each pixel corresponds to an x-ray spectrum with a net peak. This allows the easy processing of the map using the QUANTMAP© software, which by processing the maps with a set of pre-acquired standards allows to obtain quantitative maps. The maps can be expressed as apparent concentration, percent by weight, atomic percent and percent of oxides.

The operating conditions were as follows:

beam acceleration = 15 KeV, working distance = 10 mm, probe current = 5 nA. Using a process time of 1 µs; these conditions have made it possible to reach approximately 100,000 counts per second (CPS) with a dead time of 30%. The maps were acquired at a fixed magnification of 50x. Each map is the result of 8 frames with a side of about 2.55 X 1.9 mm, which involves a total scanned area of about 40 mm2. A dwell time of 7 ms was used which implies a total acquisition time of about 16 h for 8 frames scanned with a spatial resolution of 1024 * 768 pixels for a total of about 6.5 MPixel on 40 mm^2. Each set of x-ray maps was corrected for instrument probe current drift due to long acquisition times by performing an automated measurement on a reference sample of known coordinates (x, y and z) at pre-set time intervals of 1 hour.

With these maps it was possible: - evaluate the porosity, the distribution of the aggregate within the binder and identify its mineral phases; - perform a mapping to identify the value of the Hydraulic

Index of the two mortars; - obtain a modal map of the mineral phases and other components present in the mortar.

Four representative samples of original (AAM01, AAM17, AAM25, AAM37) and one samples for each phase of restoration have been chosen. The false-color X-ray maps and the amount percentages of their mineral phases are displayed in the Supplementary Material.

5. Petrographic analyses

5.1 Original Roman mortars

Based on detailed characterization by optical microscope, SEM-EDS analysis and X-ray map analysis, despite the several sampling sites all the samples have been gathered in one single group. Indeed, they show very similar grain size, sorting, composition of both aggregate and binder and A/B ratio. Furthermore, all the samples are characterized by a poor state of preservation due to the scarce amount of binder leading to the aggregate detachment.

The aggregate

The grain size of the aggregate is fine, from 0.5 to 4 mm and moderately sorted. The samples show a bimodal grain size distribution highlighted by fine and coarse grains occurring in variable ratio depending to the observed section. The clasts are spherical in shape and display a sub-angled to sub-rounded rounding. Reaction edges with the binder have not been detected. The general aspect of a thin section has been displayed in **Fig.5a** and **b**.

Petrographically, the aggregate is typically made up of lithic fragments of quartzite, micaschist, calcschist, marble and prasinite, with the only exception of mono-mineral clasts of quartz and biotite that have also been individually found.

Quartzite elements mostly have subspherical shapes and subrounded to rounded edges. They are fine and very fine-grained (**Fig.5c**).

Micaschist elements are subangular in shape and consist of lamellar micas and quartz crystals (**Fig.5d**). Some of them also contain garnet crystals (around 200 μm in size) (**Fig.5e**).

Calcschist elements are subangular in shape and consist of fine-grained carbonate, fine-grained white mica arranged in sub-millimeter and continuous oriented levels and minor fine-grained quartz (**Fig.5f**). The marble fragments show a sub-rounded to rounded shape and consist of calcite crystals with lobed edges and triple joints (**Fig.5g**).

Prasinite elements are subangular in shape and consist of lamellar chlorite, amphibole, albite and epidote crystals (**Fig.5f**).

Quartz elements are present especially in the fine-grained fraction of the aggregate. Edges can be either angular or rounded. Locally it exhibits the classic ondulose extinction due to deformation (**Fig.5g**). Biotite presents the typical lamellar shape and pleochroism from light brown to dark brown (**Fig.5h**).

Neither additions nor additives such as straw, wood or other substances have been found.

The binder

The binder, light brown in color, shows a micritic texture according to the definition of Standard UNI 11176 (NORMA UNI 11176, 2006) . It is homogeneous even though there is a widespread presence of lumps. These lumps, millimetric in size, generally have rounded shapes. They are mostly homogeneous, dark brown in color, and some of them are characterized by fractures due to the phenomenon of shrinking.

The porosity is widespread, with an irregular to rounded shape, essentially due to the detachment of the aggregate from the binder and shrinking phenomena. There is also a micro-porosity due to the loss of binder over time, which has brought the samples to their current poor state of preservation.

The Binder/Aggregate ratio is around 1/2.

5.2 Restoration mortars

Based on a detailed characterization by optical microscope, SEM-EDS analysis and X-ray map analysis, and according to archaeological data (Appolonia et al., 2010), the samples have been gathered in four groups referring to each restoration phase.

5.2.1 First restoration

Mortars of the first restoration are represented by AAM33 and AAM41 samples.

The aggregate

The grain size of the aggregate is fine (< 4 mm), in particular ranging from 200 μm to 2 mm and the grains are well sorted. The samples show a heterogeneous grain size distribution. The clasts are low-spherical and display an angular to sub-angular shape. Reaction edges with the binder have never been detected. The general aspect in thin section has been displayed in **Fig. 6a**.

Petrographically, the aggregate is made up of lithic fragments of quartzite, quartz-micaschist, chloritoschist and calcschist belonging to the coarser grain fraction (1.5 – 2 mm).

The binder

The binder is homogeneous, light brown in color and shows a micritic texture according to Standard UNI 11176 (2006).

The porosity, scarcely developed, is rounded in shape and possibly due to bubbles formation during mortar firing. The difference between this set of samples and the Roman ones is evident; the binder is very dense, little shrinking phenomena have been observed (**Fig. 6b**) but aggregate is not separating from the binder.

The Binder/Aggregate ratio is around 1\1.

5.2.2 Second restoration

Mortars of second restoration are represented by AAM34 and AAM39 samples.

The aggregate

The grain size of the aggregate is fine, from 200 µm to 2 mm in size and well sorted. The grain size distribution is heterogeneous and the samples show three grain size classes: from 200 to 400µm, from 400 to 600 and from 1 –to 2 mm evenly distributed. The clasts are sub-spherical and display a sub-angular to sub-rounded shape. Reaction edges with the binder have not been detected. The general aspect of a thin section has been provided in **Fig. 6c**.

Compositionally, the aggregate is made up of lithic fragments of micaschist, granite, marble, serpentinite, chloritoschist and aggregates of vein-filling minerals belonging to the coarse-grained fraction (1 – 2 mm). Micaschist elements are sub-angular in shape and consist of lamellar white mica and quartz crystals. Granite elements are sub-angular in shape and characterized by the following minerals: geminated K-feldspar in which albitic perthites are recognizable, quartz and albite crystals. Marble elements are rounded in shape and around 1 mm in size. Calcite crystals show the typical high birefringence and sutured edges. Serpentinite elements are made up of acicular serpentine crystals.

The clasts made up of aggregate of vein-filling minerals are typically composed by quartz, calcite, dolomite and pyrite. They show an irregular shape and are rare.

Monomineralic elements of K-feldspar have been observed. They are characterized by their typical tabular shape and they present a grain size around 2 mm.

The binder

The binder is homogeneous, dark brown in color and shows a micritic texture according to Standard UNI 11176 (2006). The porosity is widespread and characterized by rounded shape. As for the samples of the first restoration phase, the binder is very dense. Shrinking phenomena have been observed even though the aggregate is not separating from the binder.

The Binder/Aggregate ratio is around 1\1.

5.2.3 Third restoration

Mortars of the third restoration are represented by AAM35 and AAM38 samples.

The aggregate

The grain size of the aggregate is fine, from 200 µm to 2 mm, and well sorted. The samples show three grain size classes evenly distributed: from 200 to 400 µm, from 400 to 600 µm and from 1 to 2 mm. The clasts are sub-spherical and display a sub-angular to sub-rounded shape. Petrographically, the aggregate is made up by blast-furnace slags, lithic fragments of serpentinite, gneiss, calcschist, micaschist, chloritoschist and monomineralic clasts of quartz and calcite.

Blast-furnace slag displays the typical composition of this kind of material and a very characteristic morphology. Indeed, these elements, belonging to the fraction from 1 to 2 mm in size, present crystals of needle olivine surrounded by a glassy matrix. They show many rounded pores and a thick edge suggesting reaction with the binder and detachment from it. Shrinkage phenomena have also been observed around these elements (**Fig. 6e**).

Serpentinite elements are sub-rounded in shape, composed by fine-grained serpentine, and belong to the fraction around 1 mm in size. Gneiss elements are composed by albite, quartz and K-feldpar. They are sub-rounded in shape and belong to the fraction around 1 mm in size. Micaschist elements are elongated (up to 2 mm long) in shape and consist of lamellar micas and quartz crystals. Calcite elements are sub-angular in shape and belong to the fraction from 200 to 400 µm in size too.

The binder

The binder is homogeneous distributed, light to dark brown in color and shows a micritic texture according to Standard UNI 11176 (2006). The porosity is widespread and characterized by rounded in shape.

As for the samples of the first and second restoration, the binder is very dense, but in this case shrinking phenomena have been observed around the blast-furnace slags (**Fig. 6f**). On the contrary, no lumps have been observed.

The Binder/Aggregate ratio is around 1\1.

5.2.4 Fourth restoration

Mortars of fourth restoration are represented by AAM36 and AAM40 samples.

The aggregate

The grain size of the aggregate is fine, from 200 µm to 2 mm, and well sorted. The samples show three grain size classes evenly distributed: from 200 to 400 µm, from 400 to 800 µm and from 1 to 2 mm in size. The clasts are sub-spherical and display a sub-angular, sub-rounded and rounded shape. The general aspect has been provided in **Fig. 7a**.

Petrographically, the aggregate is made up of lithic fragments of granitoid, phengite-rich micaschist, calcschist, chloritoschist, rare vein-filling minerals and monomineralic clasts of quartz.

Granitoid elements are made up of quartz, plagioclase, muscovite, K-feldspar (sometimes altered) and show a sub-rounded shape. They belong to the fraction from 1 to 2 mm and to the fraction from 400 to 800 µm (**Fig. 7a**). Calcschist elements are sub-rounded in shape and consist of coarse-grained calcite, minor fine-grained quartz and crystals of white mica. They belong to the fraction from 1 to 2 mm (**Fig. 7b**). Micaschist elements are sub-rounded in shape and consist of lamellar white mica and quartz crystals.

Vein-filling minerals are composed by quartz, calcite and rare white mica, they show a sub-rounded shape and they belong to the fraction from 1 to 2 mm.

The binder

The binder, inhomogeneously distributed and characterized by light to dark brown areas, shows a micritic texture according to Standard UNI 11176 (2006).

The porosity is irregular in shape and shrinking phenomena are diffused in all sections (**Fig. 7b**).

In the binder, belite, ettringite and tetracalcium aluminoferrite occur. They are micrometer remains that had not reacted with the binder during the firing. All of them are only recognizable by SEM-EDS analysis (see Paragraph 0). Belite (**Fig. 7c**) and tetracalcium aluminoferrite are bright and

rounded in shape observed by backscattered image. Instead, ettringite is fractured and shows a circular shape that is detached from the binder (**Fig. 7d**).

The Binder/Aggregate ratio is around 1/1.

6. Mineral Chemistry

Garnet and talc have been recalculated based on 12 oxygens, pyroxene based on 6 oxygens, white mica on 11 oxygens, biotite on 22 oxygens, feldspars on 8 oxygens, chlorite on 28 oxygens, epidote on 25 oxygens. Mineral abbreviations are given according with (Whitney and Evans, 2010).

Amphibole

All the analyzed amphiboles come from the Roman mortar samples with the only exception of a single sample belonging to the third restoration (sample AAM35). The results are reported in Supplementary Material and resumed in **Fig. 8**.

The diagram Al IV vs Na(B) (**Fig. 8a**) shows the composition of all the analyzed amphiboles.

The amphiboles in the Roman samples show a variable composition as evidenced by the dispersion of the analysis points. These points are included in the field of glaucophane, actinolite, hornblende, barroisite and pargasite. The amphibole of the third restoration sample has been classified as actinolite.

All the analyzed amphiboles are classifiable as calcic or sodic-calcic amphiboles with a tremolitic to pargasitic composition, reflecting medium-low pressure and low to medium temperature metamorphic conditions. This type of amphiboles occurs in numerous units of both oceanic and continental origin outcropping in the Aosta Valley, which have suffered pervasive retrogression to low-pressure metamorphic conditions, possibly with subsequent heating stage. Sodic amphiboles, characteristic of high-pressure conditions, are absent. This data is consistent with the geographic position of the Roman Theatre, located west of the outcropping areas of the main oceanic units characterized by eclogitic facies of the Aosta Valley.

Chlorite

The analyzed chlorites come from the original samples of the Roman period and from those of the different restoration phases and have been plotted on the classification diagram of Hey (1954) (**Fig. 8b**). The analyses are reported in Supplementary Material.

The compositions of all examined chlorites are on average homogeneous. Chlorites of roman samples belong to ripidolite and pycnochlorite fields and some of them are on the limit with

diabanite, brunsvigite and ripidolite fields. Chlorites of first restoration, second and fourth samples belong to ripidolite and pycnochlorite fields. Chlorites of third restoration samples show ripidolite and brunsvigite composition.

The analyzed chlorites are typical of low metamorphic grade belonging to both the basic and pelitic systems. It is therefore a phase mineral typical of rocks from different oceanic and continental crustal units outcropping in the Aosta Valley.

Feldspar

The analyzed feldspars belong to the original samples of the Roman period and from those of the different restoration phases and refer to aggregate elements consisting of lithic fragments or single feldspar clasts. Representative analyses are plotted in the diagram of **Fig. 8c** and reported in Supplementary Material.

The composition of feldspars is variable as two main categories occur:

Albite: the feldspars of the Roman mortar samples, of the third and fourth restorations fall into this class; which is typical of the Aosta Valley rocks of low metamorphic grade from both the basic and pelitic systems.

K-feldspar: the K-feldspar of the first, second and third restoration belong to this category. The presence of K-feldspar can be attributed to the dismantling of orthogneisses (in most cases), which are widespread in the continental units of the Aosta Valley, or of granitoids (probably originating from the erosion of Mont Blanc granites).

Two feldspars of roman samples are classified as oligoclase whereas those of the second restoration show one sample between the labradorite and bytownite fields and two samples of anorthitic composition. Finally, labradorite and bytownite occur for two samples of third restoration. Intermediate to calcic composition could come from basic rocks or from high temperature units, such as the Valpelline Series, dismantled and transported downstream along the Buthier River, a left tributary of the Dora Baltea, up to the town of Aosta.

Trioctahedral Mica

The analyzed trioctahedral mica belongs to the Roman mortars and one from the fourth restoration samples. They have been plotted in the 'biotite plane' classification diagram by Guidotti. (1984) (**Fig. 8d**) and belong to the field of biotite. The analyses are shown in Supplementary Material.

The analyzed biotites were possibly part of the high-temperature metamorphic lithotypes, such as the kinzigite of the Valpelline Series, dismantled and transported downstream along the Buthier River, a left tributary of the Dora Baltea, up to the town of Aosta.

White mica

The investigated white mica crystals from the original samples of the Roman period and from those of the different restoration phases have been plotted on the Si/Al tot classification diagram. Representative analyses are reported in Supplementary Material.

The composition of this mineral varies according with two distinct classes represented in **Fig. 8e**: a first high- to medium-Si phengite (3.30-3.55 Si), a second low-Si muscovite (3.11-3.25 Si). Only samples from the third restoration show phengite exclusively. Paragonite was identified in two Roman mortar samples (analysis in Supplemetary Material).

The composition of the analyzed mica reflects high-pressure conditions, typical of the continental crustal units outcropping in Aosta Valley and, in particular, in the eclogitic facies units such as the Gran Paradiso Massif and the blue schist units of the Great Saint Bernard multinappe system.

The presence of paragonite is also typical of high-pressure continental units.

Pyroxene

The investigated pyroxene crystals come from the original samples of the Roman period and from those of first and second restoration phases and have been plotted on the classification diagrams of Morimoto (1988). The analyses can be consulted in Supplemetary Material.

The ternary classification diagram of the Ca-Fe-Mg pyroxenes by Morimoto (1988) in **Fig. 8f** allows to classify the examined clinopyroxenes.

The clinopyroxenes of the Roman samples fall into the diopside field. The pyroxenes from the first restoration vary in composition between diopside and augite. The pyroxenes from the fourth restoration sample show a predominantly augitic composition.

The analyzed pyroxenes are calcic, while the typical sodium-calcic pyroxenes of the basic rocks balanced in eclogitic conditions of the Piedmontese Zone and the sodium pyroxenes of the ortho-derivatives of the Sesia Lanzo Zone are missing. This data is consistent with the geographic position of the Roman Theatre of Aosta, located west of the outcropping areas of the main eclogitic units in the Aosta Valley. The pyroxenes could then derive from the dismantling of basic rocks of high metamorphic grade from the Valpelline Series.

7. Hydraulic Index (HI)

The Hydraulic Index is an important parameter to be referred when analyzing mortars. This index is closely related to the amount of clay minerals or hydraulic materials that is present in the starting composition of the binder.

The Roman mortar samples AAM01, AAM17, AAM25, AAM37 and the samples from the first (AAM33), second (AAM34), third (AAM35) and fourth (AAM36) restorations were selected.

Fig. 9 and **Fig. 10** show, respectively, the false-color maps of the Roman mortar samples and the different restoration phases.

Within the area of the analyzed section, the elaboration of these maps allows to better and more quickly evaluate not only the average value of the hydraulic index but also its distribution and composition, which is not always homogeneous. It also allows an easier comparison of samples of different mortars.

The Roman mortar samples present an aerial to moderately hydraulic lime binder (Mariani, 1976). In particular, the binder of sample AAM01 is quite homogeneous with values of the HI ranging between 0.00 and 0.10 that falls in the field of aerial lime. Sample AAM17 is more inhomogeneous than the previous one and mainly presents values from 0. 00 to 0.10, but it also presents areas where values ranges between 0.16 and 0.31 (in blue in the false-color HI map in **Fig. 9c**) and other areas, rarer, where this value ranges between 0.50 and 1.50 (in yellow in the false-color HI map in **Fig. 9c**). The average HI value, due to these inhomogeneities, is above 0.10, placing this binder in the field of weakly hydraulic lime.

Sample AAM25 is characterized by a low quantity of binder, however, from the histogram in **Fig. 9b** it is evident that the HI of the binder belongs to the range between 0.00 and 0.20, collocating the binder in the moderately hydraulic range.

Finally, sample AAM37, as sample AAM01, is homogeneous and the HI values fall in the range between 0.00 and 0.10; therefore, it can be defined as aerial lime.

Table 2 shows spot analyses carried out in different areas of thin sections in which binder is more abundant. They all show a calcic composition. The sample AAM01 presents HI values from 0.04 to 0.16 (Mean=0.08), the sample AAM17 from 0.01 to 0.34 (Mean=0.16), the sample AAM25 from 0.05 to 0.25 (Mean=0.17) and finally the sample AAM37 from 0.03 to 0.24 ((Mean=0.09).

The binder of the first (AAM33), second (AAM34), third (AAM35) and fourth restoration (AAM36) presents an eminently hydraulic lime (**Table 2**). They show HI values between 0.50 and 1.50.

In contrast to Roman mortars, the false-colour maps of restoration mortars show homogeneity in all samples. Also, in this case they are all calcic binders, although the % of MgO is slightly higher than Roman ones. The sample AAM33 presents HI values from 0.85 to 0.95 (Mean=0.88), the sample AAM34 from 0.87 to 1.02 (Mean=0.94), the sample AAM35 from 0.45 to 0.77 (Mean=0.58) and finally the sample AAM36 from 0.73 to 1.27 (Mean=0.87).

In **Fig. 11** it is possible to observe the comparison of the histograms of the hydraulicity index of the mortars studied. It is very evident how the Roman mortars (AAM01, AAM17, AAM25 and AAM37) have a corresponding peak around a value of 0.1, although the number of counts is different, while the restoration mortars (AAM33, AAM34, AAM35, AAM36) shift their peak towards higher hydraulicity values with a main value around 0.7. They also have a more symmetrical histogram pattern, whereas those of Roman mortars are more asymmetrical and show a Gaussian with a curve tailing towards higher values. The sample AAM35 shows a more irregular pattern probably due to the reaction edges between the binder and the slags.

8. Discussion

The results reported allow to propose archaeometric interpretations, both in strict sense and in wider-ranging terms, on the analytical study of geo-materials. Indeed, it is possible to obtain data that provide information regarding the production technology of mortars, both Roman and restoration, and regarding the supply areas of raw materials.

In order to investigate the production technology of the studied mortars, it is necessary to interpret the optical microscopy data focusing on the distribution of the aggregate elements, their shape, size and sorting. In addition, as regards the elements of the aggregate it is important to check the presence of reaction edges with the binder.

Binder data can also provide several useful information. The presence, morphology and distribution of lumps, as well as evidence of shrinking and porosity can be identified by optical microscopy and

8.1 Roman mortars

The grain size of the aggregate, from 500 μm to 4 mm, the moderate sorting and the bimodal grain size distribution highlighted by fine and coarse grains confirm the archaeological data (Appolonia, 2010) that placed the analyzed samples as bedding mortars. Furthermore, the sub-angular to sub-

rounded shape of the clasts shed light on their provenance possibly related to fluvial erosional processes.

As far as the binder is concerned, its composition and H.I. values suggest that it is a calcic aerial to moderately hydraulic lime according to Mariani et al. (1976). This type of binder is entirely in accordance with its function as a bedding material.

On the base of the distribution of H.I. in the false color maps, it will be here proposed a different interpretation of the hydraulicity classification of the studied binders, especially concerning the two samples falling on the edge across the weakly to moderate hydraulic fields (AAM17 and AAM25, respectively). Taking as main example the mortar AAM17 it is possible to observe how the more hydraulic portions (blue and yellow color in **Fig. 8c**) are strictly localized along the clasts edges and not randomly dispersed throughout the examined area. Such distribution could be related to chemical interactions between the aggregate and the binder during the mixing stage, the hardening of the mortar or both of them. On the other hand, the raw material used as lime stone (in Aosta Valley marble or calcschist) may not have been pure and therefore may have given a silicate component to the mixture. Given these assumptions, the higher hydraulicity of the samples AAM17 and AAM25 is not an intentional characteristic of their binders but, respectively, the product of subsequent processes affected the mortars or a pristine feature of the rocks adopted for the lime. As a consequence, these two binders can be classified as natural calcic aerial lime.

The widespread presence of lumps is due to a non-advanced traditional lime production technology. Indeed, the aspect and morphology of these lumps, which are often fissured, suggest that the binder is not totally mixed with the mixture, pointing to a lack of care during the mixing phase. The shrinkage phenomena observed in the binder, on the other hand, can be attributed to a shortage of binder in the mix. The widespread porosity, with an irregular to rounded shape, also indicates defects in the mixing of the mortar. Conversely, the micro-porosity is due to a loss of binder over time and bringing the samples to their current poor state of preservation.

8.2 Restoration mortars

For the restoration mortars, their difference with the ancient Roman mortars is evident. In all samples the grain size of the aggregate is finer (200 microns to 2 mm), and the distribution more homogeneous and denser. Also, the ratio binder/aggregate (B/A) is different; Roman mortars generally show a lower quantity of aggregate than restoration mortars. Indeed, the former have a B/A ratio of around 1/2 with the exception of sample AAM01 where the ratio is 2/1. Restoration mortars, on the contrary, show a quite constant ratio around 1/1 **(Table 3).**

Furthermore, in the third restoration is remarkable the presence of blast-furnace slag used in addition to lithic fragments. These slags display a very characteristic morphology. Indeed, these elements, belonging to the coarse-grained fraction (1 – 2 mm), are made up of crystals of needle olivine embedded in a glassy matrix. They show many rounded pores and a thick edge suggesting reaction processes with the binder. Shrinking phenomena have also been observed around these elements.

The binder, on the other hand, is much more compact, less degraded, and hydraulic. The H.I. value, ranging between 0.50 and 1.50, places all the restoration specimens in the range of cement mortars. Indeed, in the samples of the first, second and third restorations, the porosity, rounded in shape (**Fig. 6d**), is possibly due to bubble formation during mortar firing. Shrinking phenomena were also observed in the samples of the first and second restorations (**Fig. 6b**), which were plausibly due to the rapid hardening of the hydraulic mortars.

In the samples of the third restoration, the shrinking is not only limited to the hardening of the binder but also related to the reaction occurring between the slags and the binder itself highlighted by the occurrence of reaction edges around the individual slags (see **Fig. 6f**).

The binder used in the fourth restoration is more inhomogeneous and shows an irregular porosity. In contrast to the samples of the previous restoration phases, this is possibly due to an original lack of material during the preparation of the mortar. So that, in this case the porosity is not related to bubble formation during the firing but is a former property of the mixture. Shrinking phenomena, diffused in all samples, testify to the excessive quick hardening of the cement decreasing the mechanical performance of the material. In particular, in the binder of sample AAM36 (fourth restoration), belite, ettringite and tetracalcium aluminoferrite (C_4AF) occur. While belite and ettringite are residues that can be found in any type of cement, C_4AF is specific of Portland cement.

8.3 Supply areas

Based on Optical Microscope observations and Mineral Chemistry datait is possible to identify the supply areas of the raw materials used as aggregate in both Roman and restoration mortars. Compositionally, the aggregate of Roman mortars is made up of lithic fragments of quartzite, micaschist, calcschist, marble and prasinite with the exception of monomineralic clasts of quartz and biotite that have also been individually found. They are all lithic materials consistent with the geology of the area leading to the assumption the sources of the materials were local (**Fig. 12**).

In **Table 4** it is possible to review the main lithologies and minerals constituting the aggregate of the Roman mortars.

On the basis of the above considerations it is possible to attribute the source of supply of the raw material to the area of Aosta, it is therefore material found in close proximity to the Roman Theatre. In particular, the low amount of biotite suggest that the Romans took the material upstream of the Buthier and the Dora rivers.

It represents an important information because during Roman Age the commerce was very prosperous, and the archeologists found raw materials that coming from all over the Mediterranean area. This is an example of use of raw materials from the surrounding territory.

In **Table 5** it is possible to review the main lithologies and minerals constituting the aggregate of the restoration mortars. Considerations on the lithologies used as raw material can be made based on the mineral chemistry of the mineral phases analyzed.

For the mineral phases, in order to avoid repetitions, only the interpretation of the feldspar is given, as the others match those of Roman mortars. Indeed, plagioclase minerals with labradoritic and anorthitic composition can be referred to basic rocks or high temperature units. High-temperature basic rocks are occur in the Valpelline Series unit.

Except for the furnace slags of the third restoration, restoration mortars are all quite similar to each other. However, they are different from Roman mortars. In particular, they contain more basic and ultrabasic rocks. These could derive from the oceanic crust units of the Aosta Valley, so unlike the Roman mortars whose source of supply was close to that of the Theatre, for these mortars the raw material comes from the entire regional territory (**Fig. 12**).

9. Conclusion

The analytical protocol proposed provides an innovative method for the petrographic study of mortars. Firstly, by the observation under the optical microscope, it is possible to carry out a petrographic characterization of the mortar, both from the point of view of the aggregate and the binder. Starting from this observation, the most representative area of the sample can be identified in order to proceed with SEM-EDS quantitative mapping. From the processing of the quantitative maps, using the using the AZTEC operating system software and then processing of the map using the QUANTMAP© software, the composition of the mineral phases, their absolute abundance expressed in percentage, as well as the percentage of binder and porosity can be identified. By means of a simple algebraic operation, using the numerical matrices of the quantitative maps of Al_2O_3, Fe_2O_3 and SiO_2 with numerator and the previously acquired maps of CaO and MgO with denominator it is also possible to obtain false colors maps and the related distribution histograms of

the Hydraulicity Index. All the obtained data are useful for further analysis of the aggregate (e.g. to investigate supply areas).

In the field of the Materials Science applied to Cultural Heritage, this method is useful to provide precise information about the composition of the mortar under investigation. Its characterization allows to define several parameters that lead to a relative dating or a comparison with other samples.

Despite the poor state of preservation of the samples from the Roman period, the data obtained were satisfactory and useful for the intended purposes, namely the study of production technology and the investigation of supply areas. From the point of view of the characterization of geomaterials in a wider sense, the high level of applicability of the method is more evident for the samples of restoration mortars, which are necessarily characterized by a higher state of conservation.

This method allows to characterize the geomaterials in a way that is both expeditious and very detailed at the same time and certainly provides a complementary contribution to all those chemical and mechanical parameters that are generally used for the study of this type of material.

Acknowledgments

The research was supported by the University of Torino (ex 60% funds). It was carried out in the frame of GeoDIVE Project (M. Giardino coord.), funded by Compagnia di San Paolo Foundation and University of Torino.

Declaration of Competing Interest

The authors declare that they have no known competing financial interests or personal relationships that could have appeared to influence the work reported in this paper.

References

Appolonia L, Vaudan D, Glarey, A (2010) Lo studio delle malte del Teatro romano di Aosta: una ricerca in corso. Regione Autonoma della Valle d'Aosta, Bollettino della Soprintendenza 6: 249-252.

Bany Yaseen I. A, Al-Amoush H, Al-Farajat M, Mayyas A (2013) Petrography and mineralogy of Roman mortars from buildings of the ancient city of Jerash, Jordan, Construction and Building Materials 38: 465- 471. doi:10.1016/j.conbuildmat.2012.08.022.

Beltrando M, Compagnoni R, Lombardo B (2010) (Ultra-) high-pressure metamorphism and orogenesis: an alpine perspective. Gondwana Research, 18: 147–166.

Cannic S, Lardeaux JM, Mugnier JL, Hernandez J (1996) Tectonometamorphic evolution of the Roignais-Versoyen Unit (Valaisan domain, France). Eclogae Geologicae Helvetiae 89: 321–43.

Cantù M, Giacometti F, Landi AG, Riccardi M.P, Tarantino S C, Grimoldi A (2015) Characterization of XVIIIth century earthen mortars from Cremona (Northern Italy): Insights on a manufacturing tradition, Materials Characterization. 103: 81-89. doi:10.1016/j.matchar.2015.03.018.

Dal Piaz GV (1999) The Austroalpine-Piedmont nappe stack and the puzzle of Alpine Tethys, in Gosso G et al. (eds) Third Meeting on Alpine Geological Studies: Memorie di Scienze Geologiche, 51: 155-176.

De Giusti F, Dal Piaz GV, Massironi M, Schiavo A, (2004) Carta geotettonica della Valle d'Aosta. Mem. Sci. Geol. 55: 129-149.

Derrik MR, Stulik D, Landry JM (1999) Infrared Spectroscopy in Conservation Science. The Getty Conservation Institute, Los Angeles CA.

Elter G, Elter P (1965) Carta geologica della regione del Piccolo S. Bernardo (versante italiano): note illustrative. Memorie Istituto Geologico Mineralogico Università di Padova 25: 1–53.

Ernst W, Dal Piaz G (1978) Mineral parageneses of eclogitic rocks and related mafic schists of the Piemonte ophiolite nappe, Breuil-St. Jacques area, Italian Western Alps. American Mineralogist, 63: 621–640.

Guidotti CV (1984) Micas, Reviews in Mineralogy. Mineralogical Society of America, Chelsea.

Hey MH (1954) A new review of chlorites. Mineralogical Magazine 30: 277- 292.

Ingham JP (2013) Geomaterials Under the Microscope, Academic Press. Elsevier, Frome, UK,

Karkanas P (2007) Identification of lime plaster in prehistory using petrographic methods: A review and reconsideration of the data on the basis of experimental and case studies. Geoarchaeology 22: 775- 796. doi:10.1002/gea.20186.

Lezzerini M, Ramacciotti M, Cantini F, Fatighenti B, Antonelli F, Pecchioni E, Fratini F, Cantisani E, Giamello M (2017) Archaeometric study of natural hydraulic mortars: the case of the Late Roman Villa dell'Oratorio (Florence, Italy). Archaeol Anthropol Sci 9: 603–615. doi:10.1007/s12520-016- 0404-2

Lezzerini M, Raneri S, Pagnotta S, Columbu S, Gallello G (2018) Archaeometric study of mortars from the Pisa's Cathedral Square (Italy). Measurement126: 322-331. doi:10.1016/j.measurement.2018.05.057.

Loprieno A, Bousquet, R, Bucher S, Ceriani S, Dalla Torre FH, Fugenschuh B, Schmid SM (2011). The Valais units in Savoy (France): a key area for understanding the palaeogeography and the tectonic evolution of the Western Alps. International Journal of Earth Sciences. 100: 963-92.

Malusà MG, Polino, Martin S (2005). The Gran San Bernardo nappe in the Aosta valley (western Alps): A composite stack of distinct continental crust units. Bulletin de la Société Géologique de France 176: 417–431. doi: 10.2113/176.5.417

Mariani E (1976) I leganti aerei e idraulici. Casa Ed. Ambrosiana Milano.

Miriello D, Barca D, Bloise A, Ciarallo A, Crisci GM, De Rose T, Gattuso C, Gazineo F, La Russa MF (2010) Characterisation of archaeological mortars from Pompeii (Campania, Italy) and identification of construction phases by compositional data analysis, Journal of Archaeological Science 37: 2207-2223. doi:10.1016/j.jas.2010.03.019

Morimoto N (1988) Nomenclature of Pyroxenes. Mineralogy and Petrology 73: 1123-1133.

Moropoulou A, Theoulakis P, Chrysophakis T (1995) Correlation between stone weathering and environmental factors in marine atmosphere. Atmospheric Environment, Volume 29: 895-903.

NORMA UNI 10924 (2001) Malte per elementi costruttivi e decorativi: classificazione e terminologia. Ed UNI (Ente Nazionale Italiano Unificazione) Milano.

NORMA UNI EN 13925-1 (2006) Prove non distruttive – Diffrazione a raggi X dai materiali policristallini e amorfi – Parte 1: Principi generali. Ed. UNI (Ente Nazionale Italiano Unificazione) Milano.

NORMA UNI EN 13925-1 (2006) Prove non distruttive – Diffrazione a raggi X dai materiali policristallini e amorfi – Parte 2: Principi generali. Ed. UNI (Ente Nazionale Italiano Unificazione) Milano.

NORMA UNI EN 13925-1 (2006) Prove non distruttive – Diffrazione a raggi X dai materiali policristallini e amorfi – Parte 3: Principi generali. Ed. UNI (Ente Nazionale Italiano Unificazione) Milano.

Pecchioni E, Fratini F, Cantisani E (2018) Le malte antiche e moderne tra tradizione ed innovazione. Pàtron Editore, Seconda Edizione, Bologna

Pedelì C (2009) L'Area del teatro romano di Aosta: le attuali condizioni e le prime misure conservative., Bollettino della Regione Autonoma Valle d'Aosta 6: 242-248.

Petrakakis K, Dietrich H (1985) MINSORT: A program for the processing and archivation of microprobe analyses of silicate and oxide minerals. Neues Jahrb. Mineral. Monatshefte, 8: 379–384.

Pires J, Cruz AJ (2007) Techniques of thermal analysis applied to the study of cultural heritage. J Therm Anal Calorim 87: 411–415. https://doi.org/10.1007/s10973-004-6775-0

Riccardi MP, Lezzerini M, Carò F, Franzini M, Messiga B, (2007) Microtextural and microchemical studies of hydraulic ancient mortars: Two analytical approaches to understand pre-industrial technology process. Journal of Cultural heritage 8: 350-360.

Schiele E, Berens LW (1976) La Calce. Calcare, calce viva, idrato di calce. Ed. Tecniche ET Milano.

Von Raumer JF (1987) Les massifs du Mont Blanc et des Aiguille Rouges: temoins de la deformation de croute varisique dans les Alpes occidentales. Geologie Alpine 63: 7-24.

Whitney DL, Evans BW (2010) Abbreviations for names of rock-forming minerals. American Mineralogist, 96: 185-187.

Figures:

Fig.1 Panoramic view of the Roman Theatre of Aosta

Fig. 2 Different aspects of the Roman Theatre of Aosta: a. The area behind the cavea. b. Arches behind the façade of the theatre. c. Façade of the theatre made up of different building materials as conglomerate characterized by different granulometry and travertine. d. e. Walls constituted by pebbles. f. Wall with blocks of travertine highlighting a restoration intervention

Fig. 3 Geo-tectonic map and legend of Aosta Valley (after. De Giusti et al., 2004; modified), .

Fig. 4 a: Plan of the Roman Theatre of Aosta with the sampling areas of first (2008) and second (2009) surveys of restoration (Appolonia et al., 2010). **b:** Frontal view of the Wall 6. The colors, representing the different mortars used to build and restore the wall through time, allows to highlight the several interventions spanning from the first one dated back to the 30's to the fourth one characterized by the use of modern cement. The location of the samples AAM32, AAM33, AAM34, AAM35, AAM36, AAM37 is also illustrated

Fig. 5 Microphotographs of Roman mortars. General aspect of roman mortar by optical microscope, //pol (**a**) and X pl (**b**). Note the fine grain size of the aggregate, from 0.5 to 4 mm, moderately sorted. The clasts are sub-angled to sub-rounded rounding in shape **c**: Detail of a quartzite clast and an irregularly shaped pore (X pol). **d:** Detail of a micaschist element made up of quartz and iso-oriented white mica (X pol). **e:** Detail of a micaschist clast with a garnet crystal (SEM backscattered image). f. Detail of calcschist and prasinite clasts. Note also the irregular shape of porosity (X pol). **g**: Detail of sub-rounded clast of marble and monomineralic element of quartz with classic ondulose extinction due to deformation (X pol). h. Detail of a clast made up of single crystal of pleochroic biotite (// pol).

Fig. 6 Microphotographs of the restoration phases. **a:** General aspect of mortars by optical microscope with // Pol.. Note the fine grain size of the aggregate, 200 μm to 2 mm, which is also well sorted. The clasts are low-spherical and display an angular to sub-angular shape (First restoration). **b** Detail of thin shrinking of the binder (SEM backscattered image) (First restoration). **c:** General aspect of mortars by optical microscope, X pol. Note the fine grain size of the aggregate, 200 μm to 2 mm, with heterogeneous distribution. The clasts are sub-spherical and display a sub-angular to sub-rounded shape (Second restoration). **d:** Detail of the widespread porosity characterized by a rounded shape (SEM backscattered image) (Second restoration). **e:** Comparison of // and X Pol. images of the same mortar sample. Note the presence of blast-furnace slags, rounded lithic fragments of serpentinite and monomineralic element of quartz (Third restoration). **f:** Detail of slag with crystals of acicular olivine surrounded by a glassy matrix (SEM backscattered image) (Third restoration).

Fig. 7 Microphotographs of the fourth restoration phase. **a:** General aspect of the mortar, by optical microscope, // pol. Note the presence of granitoid lithic fragment. **b:** Detail of inhomogeneous binder characterized by lighter and darker areas as highlighted by the SEM backscattered image. **c:** Detail of bright and rounded in shape belite (SEM backscattered image). **d:** Detail of ettringite grown on original voids; note the circular shape (SEM backscattered image). Cc: calcite, Wm: white mica, Qtz: quartz.

Fig. 8 Mineral Chemistry of Roman and restoration samples. **a:** Al IV vs Na (B) classification diagram for Amphibole. **b:** Chlorite classification diagram, after Hey (1954). **c:** Feldspar ternary classification diagram. **d:** Biotite classification diagram (Guidotti, 1984) **e:** K-White Mica classification diagram. **f:** Ca-Mg-Fe Pyroxene ternary classification diagram (Morimoto, 1988).

Fig. 9 False-color maps of the Roman mortar samples and related histogram whose abscissa (500 values) shows the calculation of HI (from >0 to <10) and the ordinate all the values of the percentage calculated on the total number of pixels for each image (Freq(cnts)%). a. AAM01 sample b. AAM25 sample c. AAM17 sample d. AAM37 sample.

Fig.10 False-color maps of the restoration mortar samples and related histogram whose abscissa (500 values) shows the calculation of HI (from >0 to <10) and the ordinate all the values of the percentage calculated on the total number of pixels for each image (Freq(cnts)%). **a:** First restoration (AAM33 sample) **b:** Second restoration (AAM34 sample) **c:** Third restoration (AAM35 sample) **d:** Fourth restoration (AAM36 sample).

Fig. 11 Histograms of Roman (AAM01, AAM17, AAM25, AAM37) and restoration (AAM33, AAM34, AAM35, AAM36) mortars whose abscissa (500 values) shows the calculation of HI (from >0 to <10) and the ordinate all the values of the percentage calculated on the total number of pixels for each image (Freq(cnts)%).

Fig. 12 Geo-tectonic map of Aosta Valley, (modified after De Giusti, 2004). It is indicated the source of supply of the raw materials of Roman and Restoration mortars.

Figure1

Click here to access/download;Figure;Figure 1.tif

Figure2

Click here to access/download;Figure;Figure 2.tif

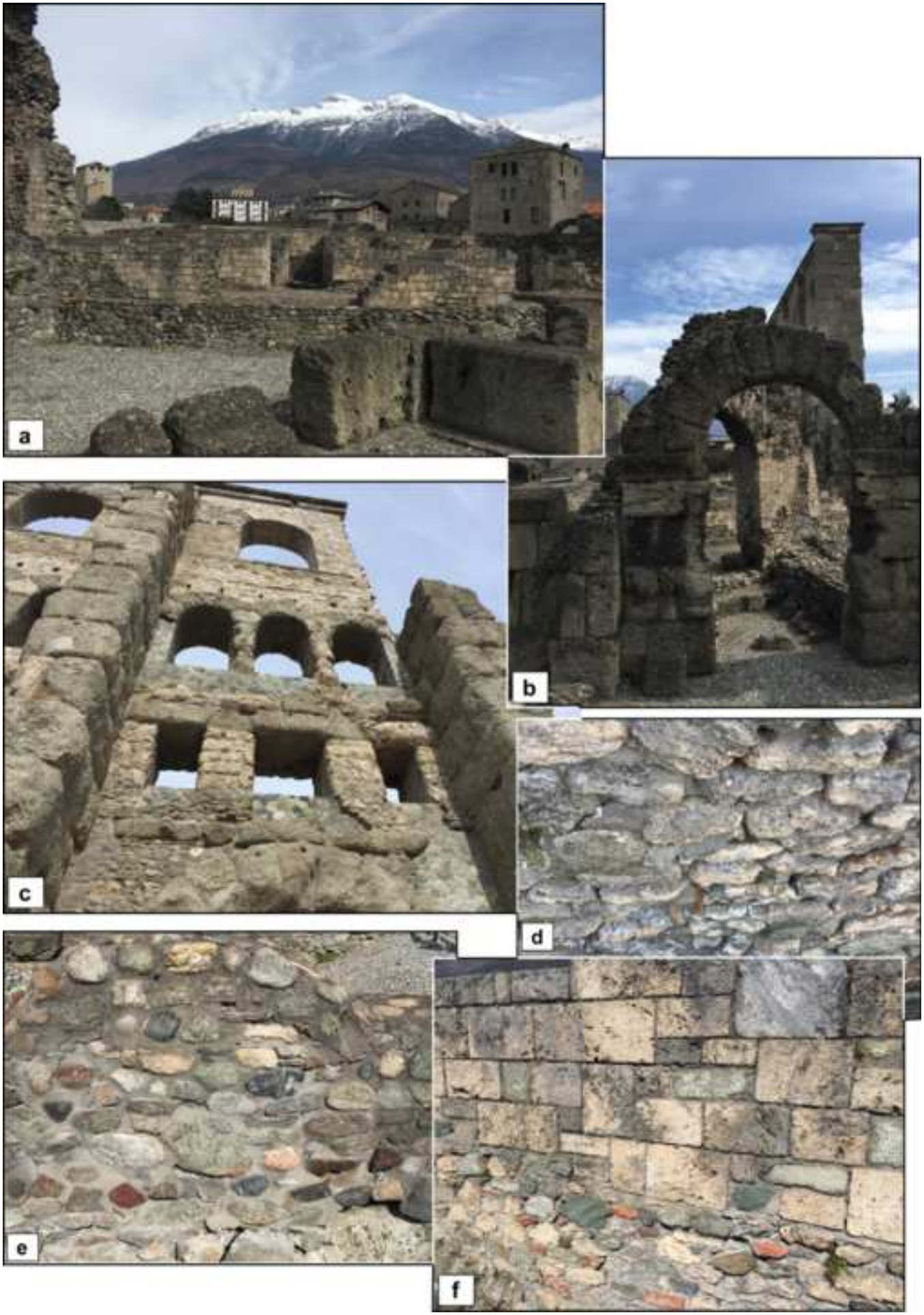

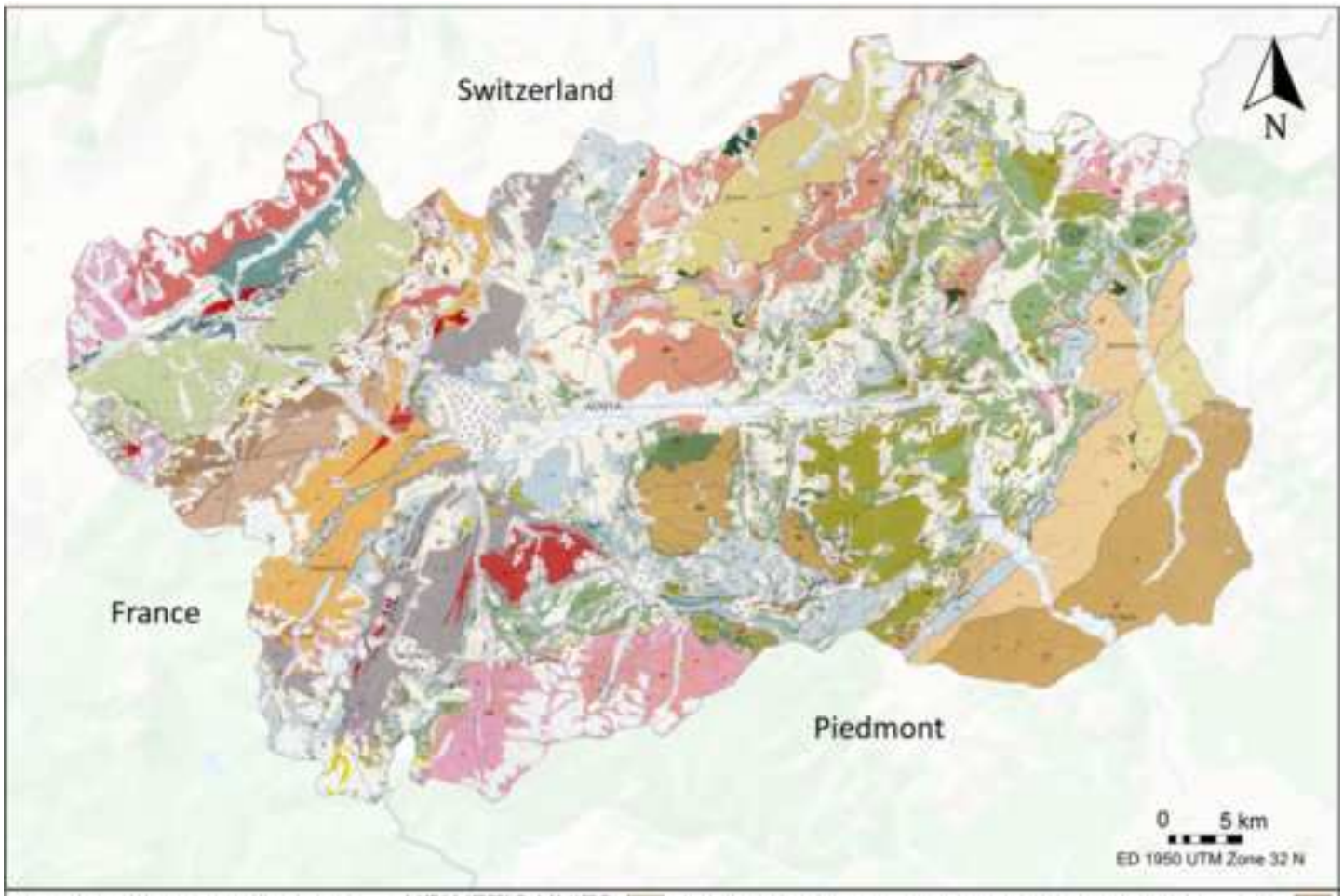

HELVETIC/ULTRAHELEVTIC - HELVETIC UNITS: 1 Undifferentiated sedimentary units (Aalenian - Albian); 2 Arenaceous-carbonaceous schist (Upper Carboniferous); Pregranitic basement: paragneiss interlayered; 3 Mont Blanc Granite; 4 with amphbolites and re-quilibrated facies. ULTRAHELVETIC UNITS - M. Chetif Unit: 5 Sedimentary unit (Early Jurassic); 6 Porfiroid and microgranite; 7 Calcschist, shale-rich schist and limestone (upper Middle Jurassic-Late Jurassic); 8 Cargneules, limestone and dolostone (Middle-Late Trias). **PENNIDIC ZONE** - EXTERNAL PENNIDIC - Sion-Courmayeur Zone 9 Flysch with conglomerate interlayers (Cretaceous); 10 Pre-Cretaceous basement: neritic Early Jurassic; gypsum, cargneules, dolostone and Triassic limestone; 11 Quartzite and conglomerate (Permian-Early Triassic); 12 Black schist and micaceous sandstone (Late Carboniferous). Versoyen Zone: 13 Prasinite; 14 Serpentinite; 15 Pelite-arenaceous calcschist; 16 Lenses of pre-Triassic quartz-micaschist. MEDIUM PENNIDIC - Piccolo San Bernardo Zone: 17 Calcschist and silceous limestone (Early Jurassic); 18 Lumachelle, carnoules and dolostone (Norian-Rhaetian). External Briançonnais: 19 Carnoules, gypsum and dolostone (Early-Middle Triassic); 20 Quartzite and conglomerate (Permian-Early Triassic); 21 Subvulcanic metagranite; 22 Conglomerate, matapsammite and metapelite (Late Carboniferous-Early Permian); 23 Schist and micaceous sandstone with antracite layers (Late Carboniferous); 24 Relicts of eclogitic and/or amphibolitic pre-alpine micaschist and gneiss with a blueschist alpine overprint; 25 Interlayers of granitic gneiss. Internal Briançonnais: 26 Phyllite marble, dark schist and breccia (Upper Cretaceous-Eocene?); 27 Limestone and dolostone (Middle Triassic); 28 Quartzite and whiteschist (Permian-Early Triassic); 29 Metagranitoid and augen-gneiss (Permian); 30 Metagranofire (Rhemes Valley, Permian); 31 Micaschist, albite-rich gneiss and graphitic schist with several interlayers of metabasite. INTERNAL PENNIDIC - Monte Rosa Nappe (MR), Arcesa Brusson Dome (AB), Gran Paradiso Nappe (GP): 32 Schist and metaconglomerate of Velleie (Permian-Carboniferous); 33 Metagranite and augen-gneiss (Permian-Carboniferous protolite); 34 High grade pre-alpine micaschist and paragneiss with eclogitic and greenschist alpine overprint. PIEDMONTESE ZONE - Combin Unit (Co) - Zermatt - Saas Unit (ZS): 35 Calcschist s.l.; 36 Greenschist, metabasalt, amphibolite and minor eclogite; 37 Metagabbro; 38 Mantle peridotite-derived serpentinite. Exotic Units (continental origin): 39 Undiffrentiated Permian-Mesozoic; successions; 40 Non ophiolitic calcschist and breccia (Early-Middle? Jurassic)

AUSTROALPINE - NON ECLOGITIC UPPER NAPPES - Dent Blanche (DB), M.Mary - Cervino (MM), Pillonet (Pi): 41 Mesozoic successions; 42 Kinzigitic complex (Valpelline Series); 43 Fine-grained orthogneiss and pre-alpine paraschist; 44 Micaschist, marble, metabasite and pegmatic dykes of Pillonet Nappe; 45 Hornblend bearing metagranite; 46 Gabbro (Permian) ECLOGITIC LOWER NAPPES - Etirol - Levaz (EL), Monte Emilius (EM), Glacier - Rafray (GR), Santanel (Sa), Tour Ponton (T), Acque Rosse (AR), Chatillon (Ch), Grun (G): 47 Gneiss Minuti Complex and greenschist re-equilibration products SESIA-LANZO ZONE: 48 Gneiss Minuti External Complex: granitic ortogneiss and minor paraderivate; 49 Eclogitic Micaschist; Complex; 50 Kinzigitic Complex (II Dioritic-Kinzigitic). POST-METAMORPHIC MAGMATISM: 51 Lamprophiric dykes (Oligocene). HYDROTHERMAL ALTERATION: - Listwenite breccia (Oligocene). QUATERNARY DEPOSITS: Glaciers Moraine deposits; Rockfall deposits; Main landslides; Alluvional deposits. LINEAR TECTONIC ELEMENTS: Main thrusts Main faults

Figure4

Click here to access/download;Figure;Figure 4.tiff

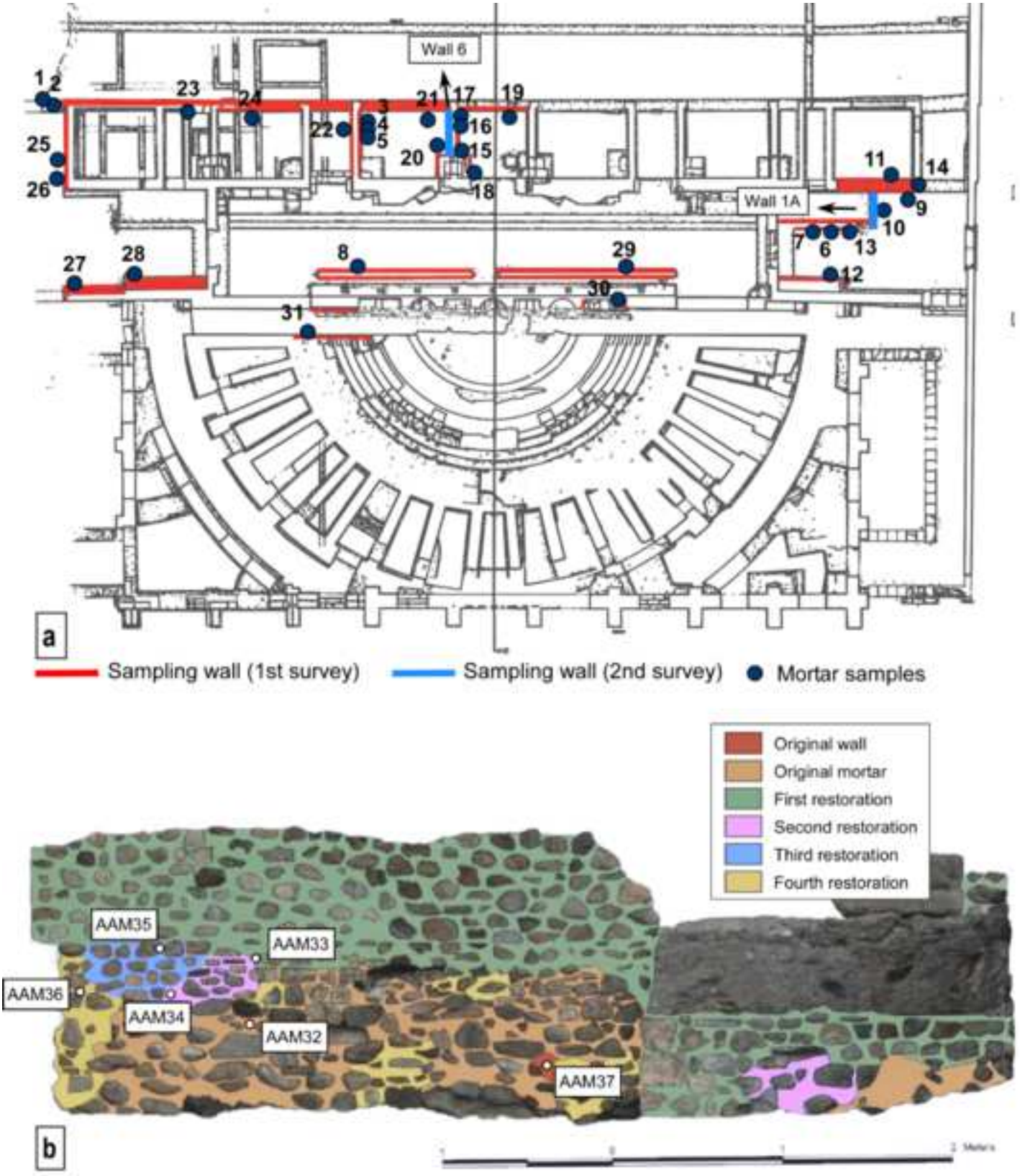

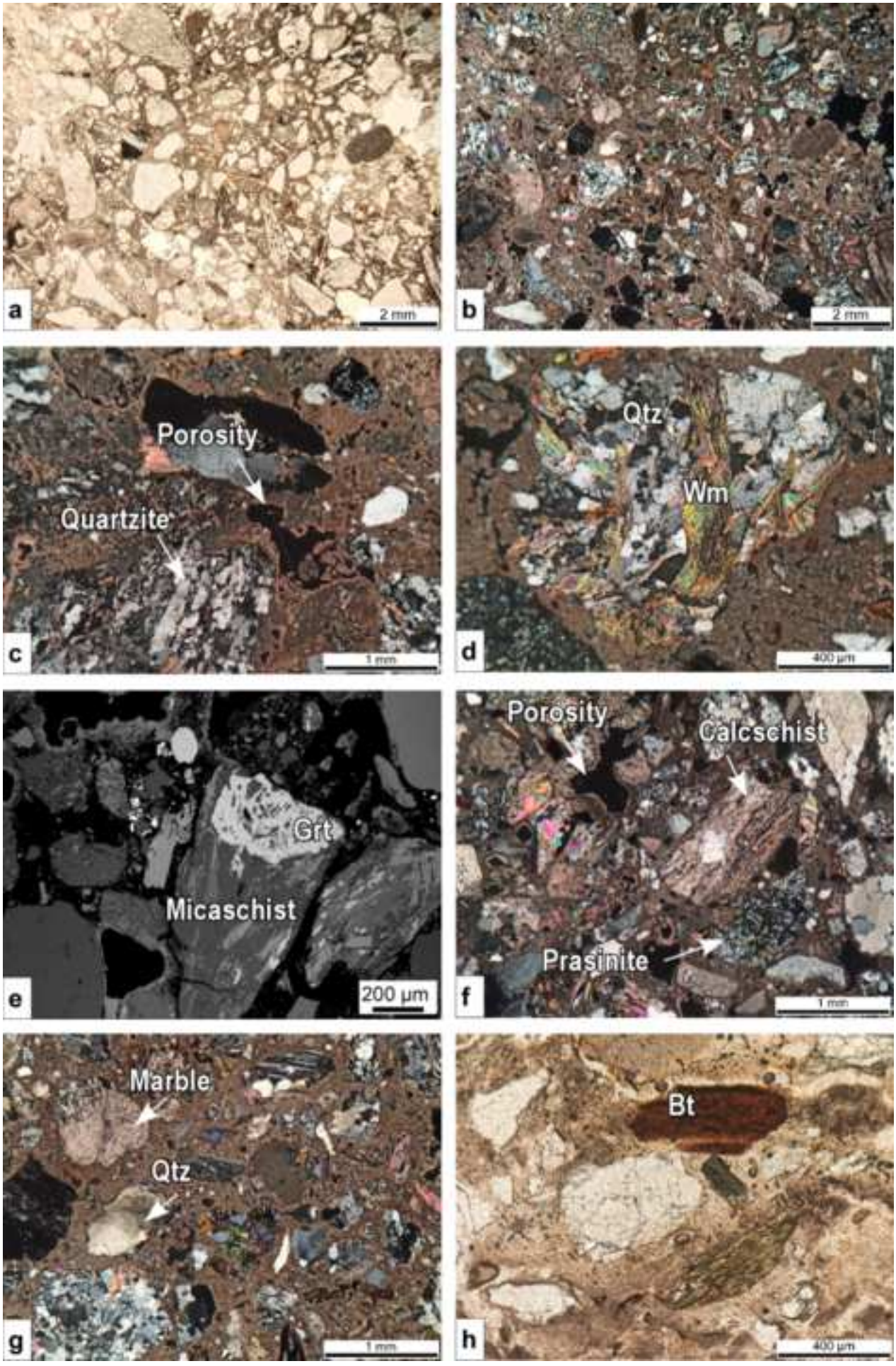

Figure6

Click here to access/download;Figure;Figure 6.tiff

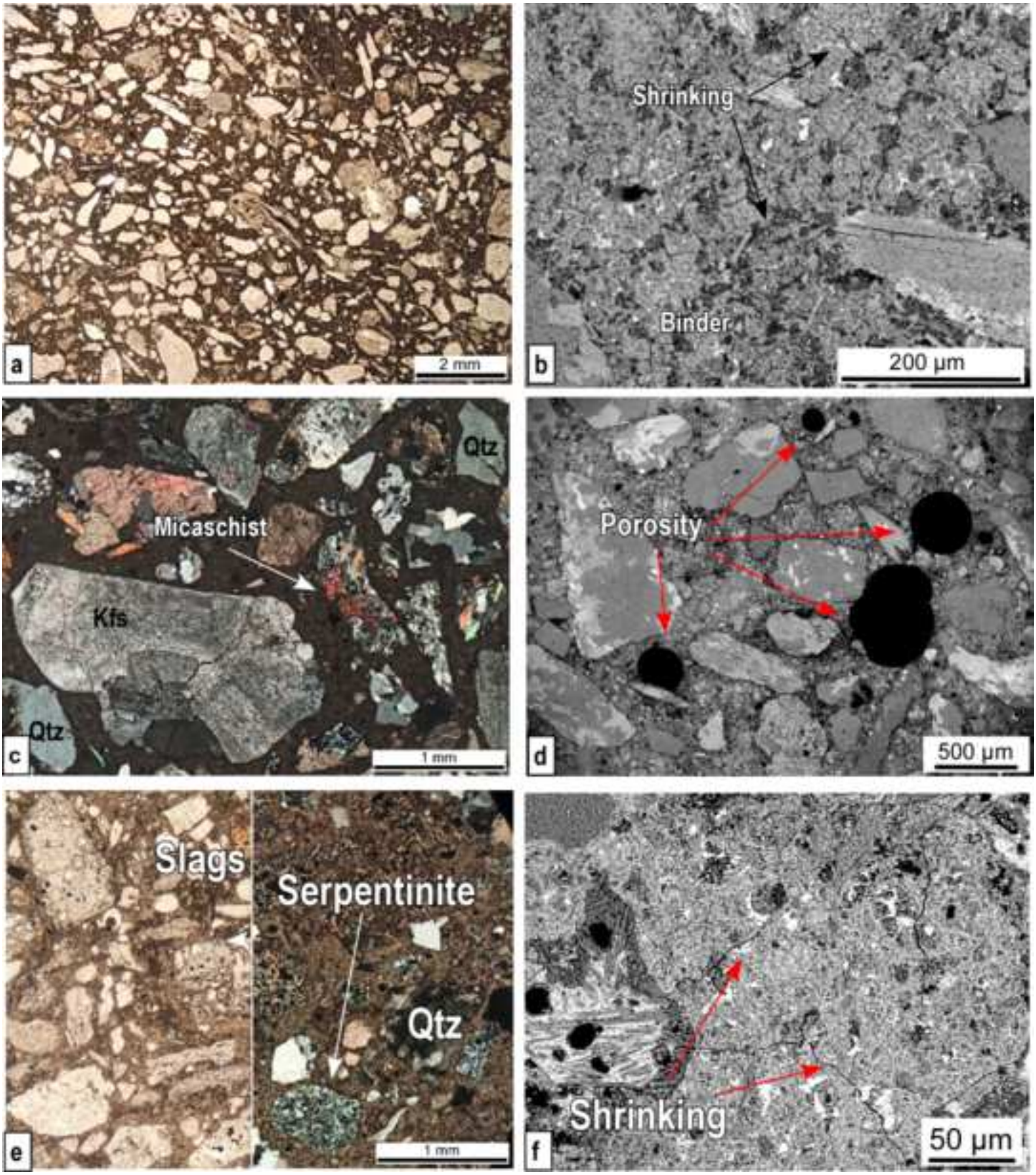

Figure7

Click here to access/download;Figure;Figure 7.tiff

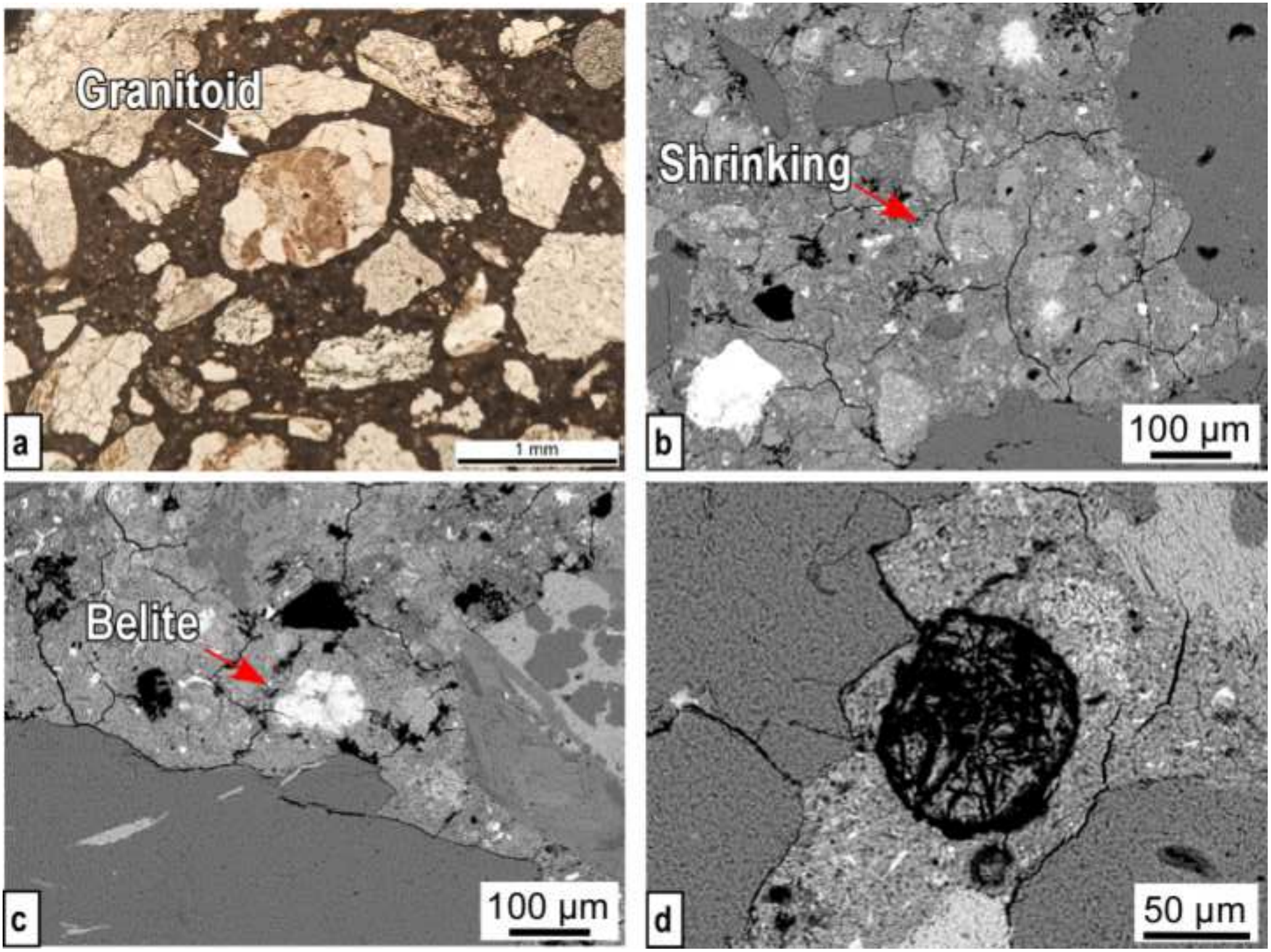

Figure8

Click here to access/download;Figure;Figure 8.tiff

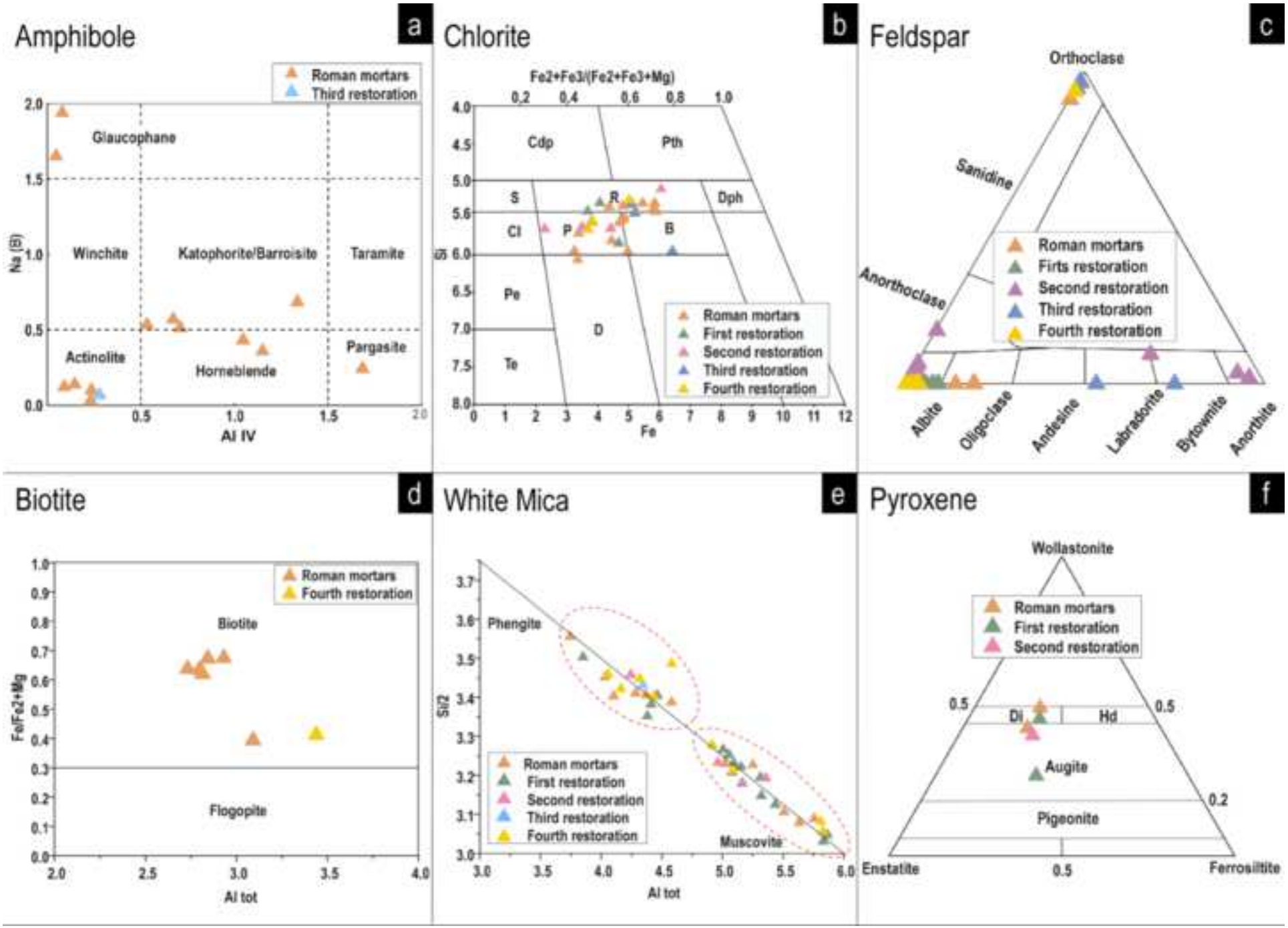

Figure9

Click here to access/download;Figure;Figure 9.tiff

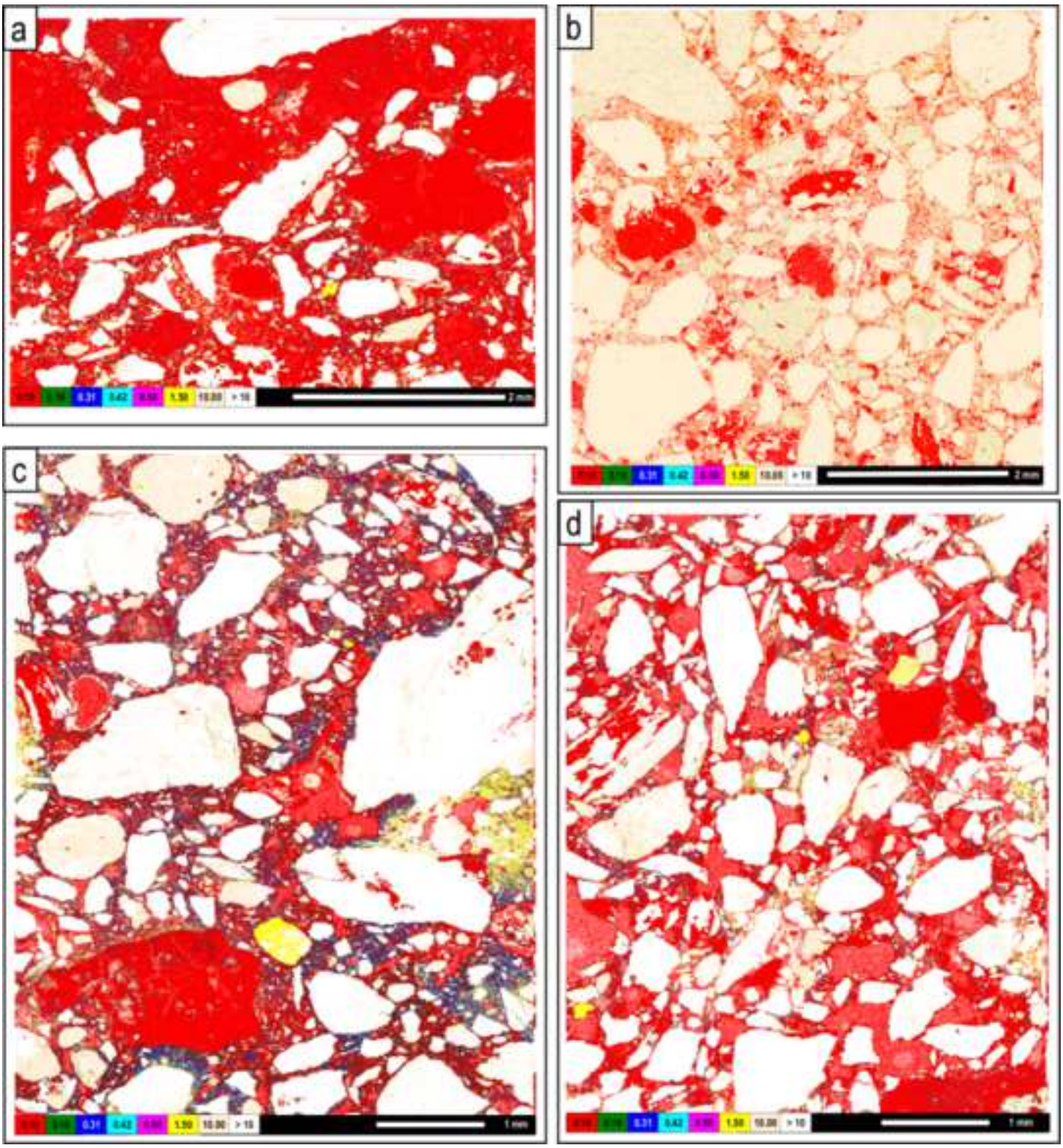

Figure10

Click here to access/download;Figure;Figure 10.tiff

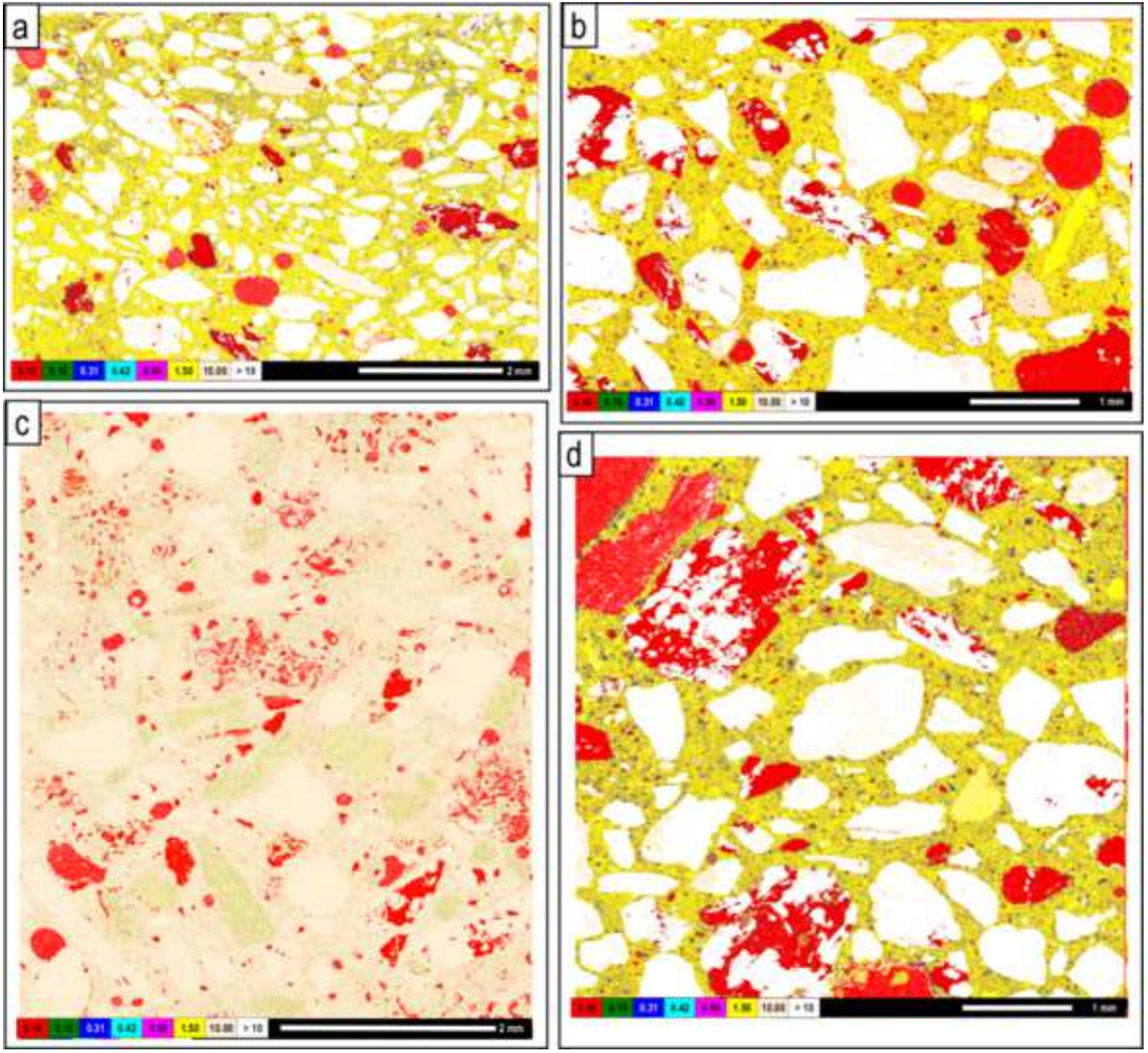

Figure11

Click here to access/download;Figure;Figure 11.tiff

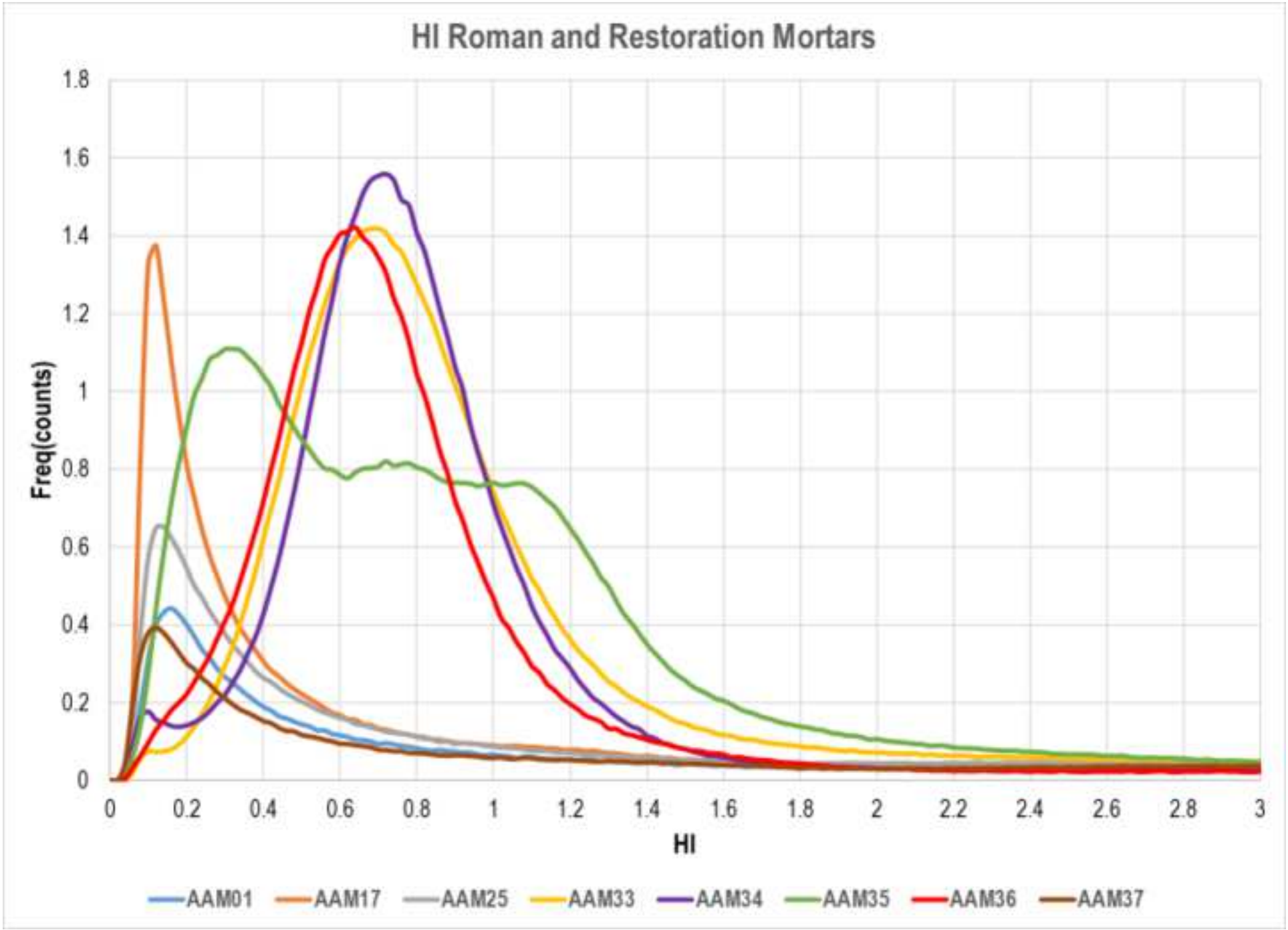

Figure12

Click here to access/download;Figure;Figure 12.tiff

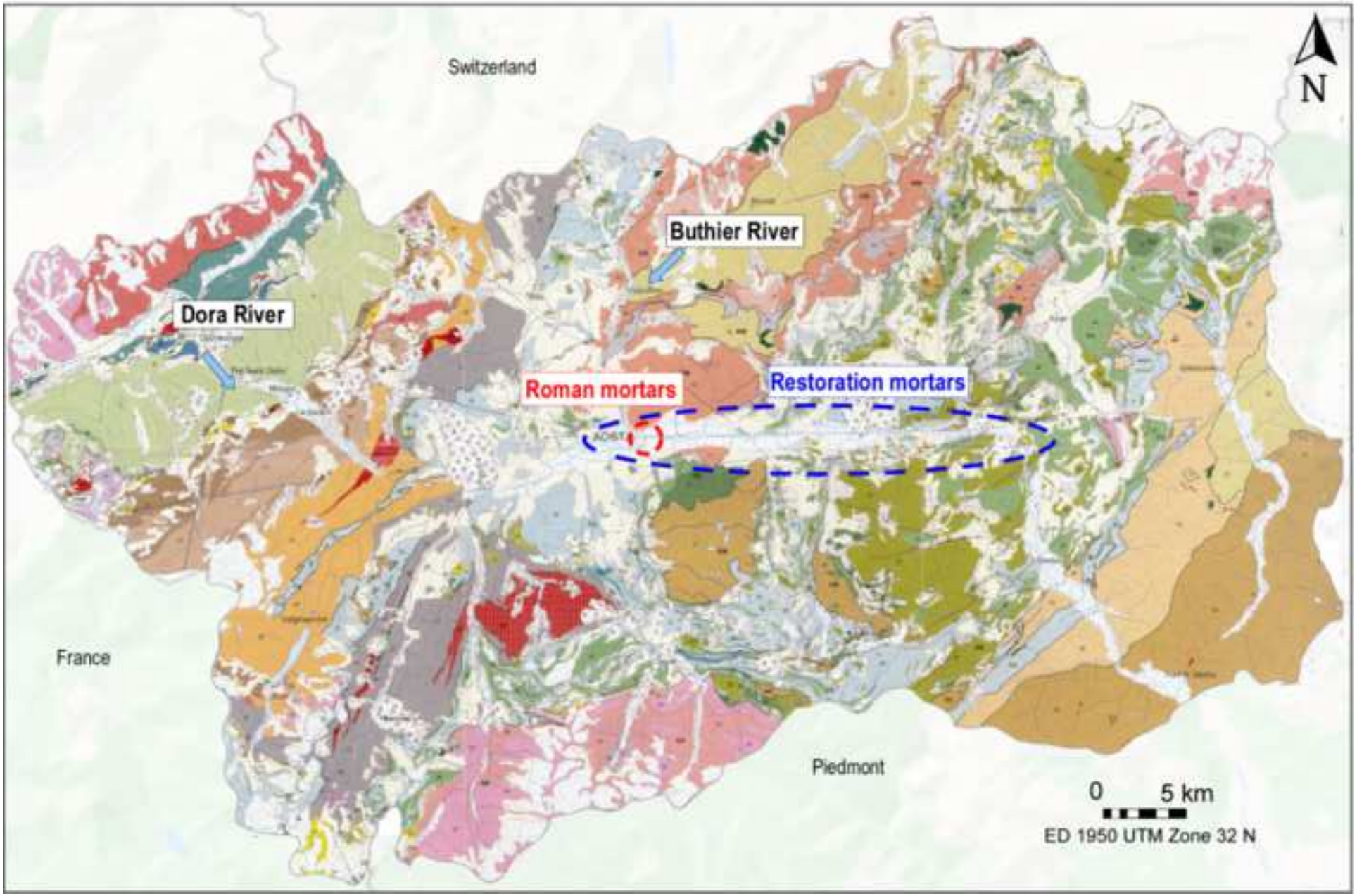

Table 1: Samples of mortars of first and second survey of restoration (from Appolonia et al., 2010).

Sample	Original/restoration mortar	Number of wall	Sample	Original/restoration mortar	Number of wall
First campaign of investigation (2008)			*First campaign of investigation (2008)*		
AAM01	Original	11	AAM23	Original	11
AAM02	Original	12	AAM24	Original	10
AAM03	Original	7	AAM25	Original	12
AAM04	Original	7	AAM26	Original	12
AAM05	Original	7	AAM27	Original	13
AAM06	Original	6	AAM28	Original	13
AAM07	Original	6	AAM29	Original	18
AAM08	Original	17	AAM30	Original	16A
AAM09	Original	1B	AAM31	Original	14
AAM10	Original	1A			
AAM11	Original	1B	*Second campaign of investigation (2009)*		
AAM12	Original	2	AAM32	Original	6
AAM13	Original	6	AAM33	First restoration	6
AAM14	Original	1B	AAM34	Second restoration	6
AAM15	Original	5A	AAM35	Third restoration	6
AAM16	Original	5A	AAM36	Fourth restoration	6
AAM17	Original	5A	AAM37	Original	6
AAM18	Original	5A	AAM38	Third restoration	1A
AAM19	Original	5B	AAM39	Second restoration	1A
AAM20	Original	6	AAM40	Fourth restoration	1A
AAM21	Original	8	AAM41	First restoration	1A
AAM22	Original	9	AAM42	Original	1A

Table2

Table 2: Representative chemical analysis of binder Roman and restoration mortars.

Sample	SiO_2	Al_2O_3	Fe_2O_3	MgO	CaO	HI
AAM01_1	9.33	2.83	1.73	1.02	85.08	0.16
AAM01_2	5.81	0.69	0.47	0.64	92.39	0.07
AAM01_3	7.38	1.1	0.92	1.39	89.22	0.10
AAM01_4	2.99	0.85	0.39	0.99	94.79	0.04
AAM01_5	3.9	0.7	0.6	0.9	93.9	0.05
AAM01_6	4.65	1.39	1.92	0.79	91.25	0.09
AAM01_7	4.47	0.76	0.71	0.52	93.54	0.06
AAM01_8	4.27	0.27	0.66	0.56	94.24	0.05
AAM01_9	5.37	2.01	1.34	0.31	90.98	0.10
AAM01_10	3.38	0.62	0.44	0.45	95.11	0.05
AAM01_11	4.09	0.73	1	0.14	94.04	0.06
Mean						**0.08**
AAM17_1	15.89	2.88	1.38	0.57	79.28	0.25
AAM17_2	5.65	1.02	0.47	0.3	92.56	0.08
AAM17_3	0.54	0.27	0.02	0.46	98.71	0.01
AAM17_4	8.52	2.3	0.74	0.51	87.93	0.13
AAM17_5	16.46	7.43	1.67	0.9	73.54	0.34
Mean						**0.16**
AAM25_1	1.59	1.15	1.82	0.86	94.58	0.05
AAM25_2	15.8	3.28	0.83	0.47	79.61	0.25
AAM25_3	10.88	1.88	0.62	0.64	85.98	0.15
AAM25_4	9.67	2.48	0.73	0.71	86.41	0.15
AAM25_5	12.53	5.7	0.64	2.18	78.96	0.23
Mean						**0.17**
AAM37_1	1.51	0.45	7.48	7.34	83.22	0.10
AAM37_2	2.78	0.96	0.25	0.11	95.9	0.04
AAM37_3	1.89	0.43	0.23	0.15	97.31	0.03
AAM37_4	3.5	1.78	0.56	0.17	93.99	0.06
AAM37_5	6.14	0.85	0.65	0.15	92.21	0.08
Mean						**0.06**

Sample	SiO_2	Al_2O_3	Fe_2O_3	MgO	CaO	HI
AAM33_1	36.78	6.4	2.66	2.54	51.62	0.85
AAM33_2	36.38	6.66	4.2	3.93	48.83	0.90
AAM33_3	39.94	5.48	2.18	3.16	49.24	0.91
AAM33_4	37.83	4.99	1.13	2.85	53.2	0.78
AAM33_5	40.11	5.29	1.54	1.55	51.51	0.88
AAM33_6	36.78	7.27	4.63	2.69	48.63	0.95
Mean						**0.88**
AAM34_1	39.99	4.74	1.87	1.75	51.66	0.87
AAM34_2	35.94	8.86	2.78	1.75	50.67	0.91
AAM34_3	37.61	8.59	2.79	1.49	49.52	0.96
AAM34_4	36.99	8.05	5.46	2.57	46.93	1.02
AAM34_5	36.04	8.94	3.58	1.52	49.93	0.94
AAM34_6	35.44	9.48	3.64	2.09	49.35	0.94
Mean						**0.94**
AAM35_1	28.94	5.03	2.7	3.29	60.03	0.58
AAM35_2	24.17	4.41	2.47	3.82	65.13	0.45
AAM35_3	31.28	3.33	2.41	4.53	58.46	0.59
AAM35_4	23.39	4.47	2.14	2.47	67.53	0.43
AAM35_5	30.48	6.07	2.1	3.22	58.14	0.63
AAM35_6	32.36	8.19	2.88	3.85	52.72	0.77
AAM35_7	29.96	4.58	2.57	3.21	59.68	0.59
Mean						**0.58**
AAM36_1	31.75	8.23	2.26	1.94	55.82	0.73
AAM36_2	35.68	6.6	3.53	1.83	52.35	0.85
AAM36_3	38.11	6.37	2.05	2.37	51.09	0.87
AAM36_4	33.29	9.21	2.28	2.16	53.06	0.81
AAM36_5	34.06	7.03	4.24	2.1	52.57	0.83
AAM36_6	31.49	7.92	3.44	2.14	55.01	0.75
AAM36_7	40.12	13.57	2.31	1.37	42.63	1.27
Mean						**0.87**

Table3

Table 3: Percentage of binder, aggregate, porosity and ratio B/A of Roman and restoration mortars.

	Samples	Binder (%)	Aggregate (%)	Porosity (%)	Ratio B/A
Roman mortars	AAM01	59	34	7	2/1
	AAM17	34	60	6	1/2
	AAM25	37	60	3	1/2
	AAM37	20	57	23	1/2
Restoration mortars	AAM33 (1° rest.)	51	43	6	1/1
	AAM34 (2° rest.)	40	47	13	1/1
	AAM35 (3° rest.)	45	51	4	1/1
	AAM36 (4° rest.)	44	47	9	1/1

Table4

Table 4: Main lithologies and minerals constituting the aggregate of the Roman mortars.

Sample	QTZ	WM	BT	Quartzite	Plagio clase	KFS	Gneiss	Marble	Calcs chist	Mica schist	Garnet	Chlorito schist	Serpen tinite	Prasinite
Roman mortars														
AAM01	x	x	x	x	x	x		x	x	x				x
AAM02	x	x	x	x	x	x					x			
AAM03	x	x	x	x	x	x								
AAM04		x		x	x	x								
AAM05	x	x		x	x	x								x
AAM06	x	x	x	x	x	x					x			
AAM07	x	x	x	x	x						x			
AAM08	x	x		x	x						x			
AAM09	x	x	x	x	x	x								
AAM10	x	x	x	x	x	x								
AAM11	x	x	x	x	x	x								x
AAM12	x	x	x	x	x	x								
AAM13		x	x	x	x	x								
AAM14	x	x		x	x									
AAM15	x	x		x	x	x								
AAM16		x	x	x	x	x					x			
AAM17	x	x	x	x	x	x								
AAM18	x	x		x	x	x								
AAM19	x	x	x	x	x									
AAM20	x	x	x	x	x	x								
AAM21	x	x	x	x	x									
AAM22		x		x	x									x
AAM23	x	x	x	x	x									
AAM24	x	x	x	x	x	x								
AAM25	x	x	x	x	x	x					x			
AAM26	x	x		x	x	x					x			x
AAM27	x	x	x	x		x					x			
AAM28	x	x		x	x	x								
AAM29	x	x	x	x	x	x								x
AAM30	x	x	x	x	x	x					x			
AAM31	x	x		x	x	x								
AAM32	***x***	x		x	x	x								
AAM37	x	x	x	x	x	x					x			x
AAM42	x	x	x	x	x									

Table5

Table 5: Main lithologies and minerals constituting the aggregate of the restoration mortars.

Sample	Quartz	White mica	Biotite	Quartzite	Plagioclase	K-feldspar	Gneiss	Marble	Calcschist	Micaschist	Garnet	Chloritoschist	Serpentinite	Prasinite	Granitic rocks	Vein filling minerals	Slags
First restoration																	
AAM33	x			x	x	x			x	x		x					
AAM41	x			x	x	x			x	x		x					
Second restoration																	
AAM34	x	x				x		x		x			x		x	x	
AAM39	x	x				x		x		x			x		x	x	
Third restoration																	
AAM35	x					x			x	x		x	x				x
AAM38	x					x			x	x		x	x				x
Fourth restoration																	
AAM36	x	x	x			x			x	x					x	x	
AAM40	x	x				x			x	x					x	x	

Supplementary Material figure

Supplementary Material analyses